spectroscopy analysis revealed that the calcified lesion consisted only of CPPD, not hydroxyapatite (Fig. 4d).

After the surgical treatment, the patient quickly recovered from neurological deterioration. At the latest follow-up, 2 years after the surgery, the patient was doing well and had no neurological deterioration. Postoperative CT revealed complete resection of the calcification of the posterior atlantoaxial membrane (Fig. 2c, d). No obvious instability and progression of OPLL were observed in dynamic X-rays of the cervical spine.

Written informed consent was obtained from the patient to publish this case report and any accompanying images.

Discussion

The first case of myelopathy due to CLF at the cervical spine was described in the late 1970s [3, 4]. Since those reports, to the best of our knowledge, more than 100 cases of symptomatic cervical CLF have been reported. The overwhelming majority of these cases have been reported from Japan. We have summarized the data available from previously reported cases in Table 1. This entity is more prevalent in elderly females [1, 5].

Theoretically speaking, CLFs can arise from any level of the cervical spine; but they predominantly arise from the lower cervical spine, with the two most commonly affected levels being C4/5 and C5/6 (Table 1). To the best of the authors' knowledge, Inoue et al. [6] briefly reported the first case of calcification of the posterior atlantoaxial membrane. The case was a 42-year-old man without any systemic background for ectopic ossification, yet he displayed multiple-level cervical ossification of the ligamentum flavum (OLF), thoracic OPLL, cervical CLF, and calcification of the posterior atlantoaxial membrane. However, the authors did not perform a detailed crystallographic analysis of the calcification of the posterior atlantoaxial membrane. Although the present case is the second report of calcification of the posterior atlantoaxial membrane, this is the first to include a crystallographic analysis.

The precise pathophysiology of CLF remains unknown; however, elastic fibers undergoing breakdown (i.e., degenerative changes in the ligamentum flavum) have been reported to exhibit increased affinity for calcium [7, 8]. It is commonly recognized that degenerative changes in the ligamentum flavum are induced by a combination of various factors, including the aging process, the decrease in estrogen in elderly women, mechanical stress of the lower cervical spine [7, 8], and chondrocytic metaplasia [9].

There have been no previous reports on calcification of the posterior atlantoaxial membrane. Functionally speaking, the ligamentum flavum provides a static, elastic force to support the spinal column in its return to a neutral position after flexion and extension movements. In turn, the posterior atlantoaxial membrane predominantly consists of a collagenous tissue, while elastic fibers comprise a minor counterpart [10]. Macroscopically, Ramsey [10] reported a definite lack of yellow color in these two upper cervical ligaments attached to the laminae of C1 and C2. On microscopic examination of the posterior atlantoaxial membrane

Table 1 Age distribution and topographic and crystallographic characterization of the 33 previously reported papers on the calcification of ligamentum flavum, along with a list of those papers

	Cervical segment						
	C1/2	C2/3	C3/4	C4/5	C5/6	C6/7	C7/T1
Distribution of calcium deposits	1	5	37	62	71	36	8
	Crystal type						
	CAP		CPPD	CPPD + HAP		HAP	Others
Number of identified calcium deposits	2		63	15		22	2
	Patient's age group						
	40s		50s	60s			Over 70
Female/total number	2/2		4/9	29/35			43/57

(1) Nanko et al. [14][a], (2) Kamakura et al. [4], (3) Jyotoku and Harada [16][a], (4) Kawano et al. [17], (5) Kida and Tabata [18][a], (6) Nagashima et al. [19][a], (7) Fujiwara et al. [20][a], (8) Akino et al. [15][a], (9) Iwasaki et al. [11], (10) Nakajima et al. [7], (11) Nagashima et al. [37], (12) Ogata et al. [12], (13) Hirano et al. [21][a], (14) Berghausen et al. [22], (15) Kubota et al. [23], (16) Kawano et al. [24], (17) Koyama et al. [38][a], (18) Hankey et al. [25], (19) Gomez and Chou [26], (20) Sato et al. [27], (21) Ohnishi et al. [28][a], (22) Okada et al. [8], (23) Takayama et al. [29][a], (24) Baba et al. [5], (25) Haraguchi et al. [30][a], (26) Higashi et al. [31][a], (27) Yamagami et al. [32], (28) Cabre et al. [13], (29) Ugarriza et al. [33], (30) Guesmi et al. [34], (31) Muthukumar and Karuppaswamy [35], (32) Yabuki and Kikuchi [36], (33) Mwaka et al. [9]

CAP carbonate apatite, *CPPD* calcium pyrophosphate dihydrate, *HAP* hydroxy apatite

[a] Articles in Japanese

in adults, the concentration of elastic fibers is approximately half that seen in true ligamentum flavum. These differences may contribute to the discrepant prevalence of CLF and calcification of the posterior atlantoaxial membrane.

Some authors have assumed a possible association between CLF and articular chondrocalcinosis (pseudogout) [5]. The generalized articular chondrocalcinosis seen in the present case led us to hypothesize that, at least in part,chondrocalcinosis played a role in the calcification of the posterior atlantoaxial membrane. The unusual mechanical stress that converged on C1/2 due to the mixed-type OPLL extending from C2 to C5 in the present case may also have played a significant role in this condition.

The etiology of CLF is likely to be different from that of OLF [1]; however, Inoue et al. [6] suggested the possibility that the same factor may have initiated ossification and calcification in spinal ligaments. Further studies are needed to elucidate the pathophysiology of calcification and ossification of the spinal ligaments.

Standard X-rays can show abnormal shadows of calcification on the posterior wall of the spinal canal [11]. However, these sometimes fail to demonstrate any abnormality other than mild spondylosis [12]. MR imaging is useful for identifying spinal cord and/or nerve root involvement; however, it cannot distinguish between calcification and hypertrophied (uncalcified) spinal ligaments since these two conditions both yield low intensity on the T1- and T2-weighted images. On the other hand, CT can clearly differentiate between these two conditions and is the best modality for detecting calcification of the spinal ligaments [13].

The natural history of cervical myelopathy due to CLF is not fully understood, since most of the previously reported cases were treated surgically. However, Cabre et al. [13] reported conservative treatment of two cases; i.e., one declined surgery and the other one had cardiorespiratory disease contraindicating surgery. These two cases uniformly worsened neurologically, whereas surgical treatment has achieved good results in most previous reports [5, 13]. Taking all of these findings into account, surgical treatment was advocated in symptomatic patients with cervical CLF [13]. One can perhaps extend this surgical indication to include calcification of the posterior atlantoaxial membrane.

In conclusion, calcification of the posterior atlantoaxial membrane is an extremely rare disease. We must to keep in mind the possibility of latent calcification of the cervical spinal ligaments in patients with generalized articular calcification. When symptomatic, surgical treatment is advocated to prevent further neurological compromise.

Acknowledgments This study was supported by Health and Labour Science Research Grants. No other financial associations were relevant or may be seen as relevant to the submitted manuscript. The authors thank Dr. Mitsuaki Ishida, Department of Clinical Laboratory Medicine, Shiga University of Medical Science, for histopathological assistance.

Conflict of interest The authors declare that they have no conflict of interest.

References

1. Miyasaka K, Kaneda K, Sato S, Iwasaki Y, Abe S, Takei H, Tsuru M, Tashiro K, Abe H, Fujioka Y. Myelopathy due to ossification or calcification of the ligamentum flavum: radiologic and histologic evaluations. AJNR Am J Neuroradiol. 1983;4(3):629–32.
2. Imai S, Hukuda S. Cervical radiculomyelopathy due to deposition of calcium pyrophosphate dihydrate crystals in the ligamentum flavum: historical and histological evaluation of attendant inflammation. J Spinal Disord. 1994;7(6):513–7.
3. Ellman MH, Vazquez T, Ferguson L, Mandel N. Calcium pyrophosphate deposition in ligamentum flavum. Arthritis Rheum. 1978;21(5):611–3.
4. Kamakura K, Nanko S, Furukawa T, Mannen T, Toyokura Y. Cervical radiculomyelopathy due to calcified ligamenta flava. Ann Neurol. 1979;5(2):193–5.
5. Baba H, Maezawa Y, Kawahara N, Tomita K, Furusawa N, Imura S. Calcium crystal deposition in the ligamentum flavum of the cervical spine. Spine (Phila Pa 1976). 1993;18(15):2174–81.
6. Inoue H, Seichi A, Kimura A, Endo T, Hoshino Y. Multiple-level ossification of the ligamentum flavum in the cervical spine combined with calcification of the cervical ligamentum flavum and posterior atlanto-axial membrane. Eur Spine J. 2013;22(Suppl 3):S416–20.
7. Nakajima K, Miyaoka M, Sumie H, Nakazato T, Ishii S. Cervical radiculomyelopathy due to calcification of the ligamenta flava. Surg Neurol. 1984;21(5):479–88.
8. Okada G, Hosoi S, Kato K, Ohta K, Tachi Y, Sonoda J, Yada H. Case report 779. Carbonate apatite calcification of ligamentum flavum. Skeletal Radiol. 1993;22(3):211–3.
9. Mwaka ES, Yayama T, Uchida K, Kobayashi S, Kokubo Y, Nakajima H, Sato R, Orwotho NT, Baba H. Calcium pyrophosphate dihydrate crystal deposition in the ligamentum flavum of the cervical spine: histopathological and immunohistochemical findings. Clin Exp Rheumatol. 2009;27(3):430–8.
10. Ramsey RH. The anatomy of the ligamenta flava. Clin Orthop Relat Res. 1966;44:129–40.
11. Iwasaki Y, Akino M, Abe H, Tsuru M, Tashiro K, Miyasaka K, Kaneda K, Isu T, Ito T. Calcification of the ligamentum flavum of the cervical spine. Report of four cases. J Neurosurg. 1983;59(3):531–4.
12. Ogata M, Ishikawa K, Ohira T. Cervical myelopathy in pseudogout. Case report. J Bone Joint Surg Am. 1984;66(8):1301–3.
13. Cabre P, Pascal-Moussellard H, Kaidomar S, Bucki B, Bardin T, Smadja D, Arfi S. Six cases of cervical ligamentum flavum calcification in Blacks in the French West Indies. Joint Bone Spine. 2001;68(2):158–65.
14. Nanko S, Takagi A, Mannen T, et al. A case of radiculo-myelopathy due to calcification of the ligamentum flavum. Shinkeinaika. 1976;4(3):205–10 (in Japanese).
15. Akino M, Abe H, Iwasaki Y, Hokin K, Tsuru M, Koiwa M, Saito H. Case of cervical myelopathy due to calcified mass in the cervical yellow ligament. No Shinkei Geka. 1983;11(2):173–8.
16. Jyotoku Z, Harada H. A case of cervical myelopathy due to calcification of the ligamentum flavum. Rinsho Seikei Geka. 1980;15(7):708–12 (in Japanese).
17. Kawano N, Yoshida S, Ohwada T, Yada K, Sasaki K, Matsuno T. Cervical radiculomyelopathy caused by deposition of calcium pyrophosphate dihydrate crystals in the ligamenta flava. Case report. J Neurosurg. 1980;52(2):279–83.

18. Kida H, Tabata S. Calcified mass in the cervical ligament flava as a cause of cervical myelopathy. Rinsho Seikei Geka. 1981;16(3):310–3 (in Japanese).
19. Nagashima C, Takahama M, Shibata K, et al. CPPD crystal deposition in the cervical ligament flava producing cervical myelopathy with special reference to the scanning electron microscopic and X-ray microanalytic studies. J Saitama Med School. 1981;8(1,2):33–45 (in Japanese).
20. Fujiwara M, Bitoh S, Hasegawa H, Nakata M, Hata H. A case of nodular calcification of the ligamentum flavum with ossification of the posterior longitudinal ligament in the cervical spine. No Shinkei Geka. 1982;10(7):769–74 (in Japanese).
21. Hirano H, Nakanishi K, Mimatsu K, et al. Myelopathy due to calcium deposition in the cervical ligament flava. Report of two cases. Cent Jpn J Orthop Traumat. 1985;28(1):447–9 (in Japanese).
22. Berghausen EJ, Balogh K, Landis WJ, Lee DD, Wright AM. Cervical myelopathy attributable to pseudogout. Case report with radiologic, histologic, and crystallographic observations. Clin Orthop Relat Res. 1987;214:217–21.
23. Kubota T, Kawano H, Yamashima T, Ikeda K, Hayashi M, Yamamoto S. Ultrastructural study of calcification process in the ligamentum flavum of the cervical spine. Spine. 1987;12(4):317–23.
24. Kawano N, Matsuno T, Miyazawa S, Iida H, Yada K, Kobayashi N, Iwasaki Y. Calcium pyrophosphate dihydrate crystal deposition disease in the cervical ligamentum flavum. J Neurosurg. 1988;68(4):613–20.
25. Hankey GJ, Khangure MS. Cervical myelopathy due to calcification of the ligamentum flavum. Aust N Z J Surg. 1988;58(3):247–9.
26. Gomez H, Chou SM. Myeloradiculopathy secondary to pseudogout in the cervical ligamentum flavum: case report. Neurosurgery. 1989;25(2):298–302
27. Sato K, Hayashi M, Kubota T, Kawano H, Handa Y, Kabuto M. Symptomatic calcification and ossification of the cervical ligamentum flavum: clinical, radiological and pathological features. Br J Neurosurg. 1989;3(5):597–602.
28. Ohnishi H, Kurihara A, Uratsuji M, et al. Three cases of cervical myelopathy due to calcification of yellow ligament. Seikeigeka. 1992;43(5):655–60 (in Japanese).
29. Takayama S, Kuribayashi K, Miyamoto Y, Nakasu Y, Handa J. Ossification and calcification of the cervical ligamentum flavum—case reports. No To Shinkei. 1993;45(9):859–63 (in Japanese).
30. Haraguchi K, Yamaki T, Kurokawa Y, Ohtaki M, Ibayashi Y, Uede T, Tanabe S, Hashi K. A case of calcification of the cervical ligamentum flavum. No Shinkei Geka. 1996;24(1):69–73 (in Japanese).
31. Higashi S, Hamada J, Ono W, Tamai K, Saotome K. Calcification of cervical ligamentum flavum—analysis of calcium compounds and histopathological findings. Ryumachi. 1997;37(6):794–803 (in Japanese).
32. Yamagami T, Kawano N, Nakano H. Calcification of the cervical ligamentum flavum—case report. Neurol Med Chir (Tokyo). 2000;40(4):234–8.
33. Ugarriza LF, Cabezudo JM, Porras LF, Rodríguez-Sánchez JA. Cord compression secondary to cervical disc herniation associated with calcification of the ligamentum flavum: case report. Neurosurgery. 2001;48(3):673–6.
34. Guesmi H, Lamouchi T, Mlaiki A, Ksira I, Tlili K, Krifa H. Calcification of the cervical ligamentum flavum. Case report and review of the literature. Neurochirurgie. 2005;51(6):591–4 (in French).
35. Muthukumar N, Karuppaswamy U. Tumoral calcium pyrophosphate dihydrate deposition disease of the ligamentum flavum. Neurosurgery. 2003;53(1):103–8
36. Yabuki S, Kikuchi S. Endoscopic surgery for cervical myelopathy due to calcification of the ligamentum flavum. J Spinal Disord Tech. 2008;21(7):518–23.
37. Nagashima C, Takahama M, Shibata T, Nakamura H, Okada K, Morita H, Kubo H. Calcium pyrophosphate dihydrate deposits in the cervical ligamenta flava causing myeloradiculopathy. J Neurosurg. 1984;60(1):69–80
38. Koyama S, Nishimura T, Kubokura T, Sannoh N, Tsubone K. A case of myelopathy caused by calcified nodules of cervical ligamentum flavum. No Shinkei Geka. 1988;16(10):1179–85 (in Japanese).

最新原著レビュー

胸部CTからみた胸椎黄色靱帯骨化症の有病率，分布と形態[1)]

森　幹士*

原題　*Mori K, Kasahara T, Mimura T et al : Prevalence, distribution, and morphology of thoracic ossification of the yellow ligament in Japanese ; results of CT-based cross-sectional study. Spine 38 : E1216-E1222, 2013*

[整形外科 65巻13号：1382～1384，2014]

【要　旨】

目　的：胸部コンピュータ断層撮影（CT）検査結果から，胸椎黄色靱帯骨化症（OYL）の有病率，分布と形態を調査すること．

方　法：胸部疾患またはその疑いのために当院を受診し，胸部CT検査を受けた連続例を対象とした．胸椎手術の既往歴があるもの，15歳以下のものは除外した．胸部CTデータを骨条件に変換し，OYLの有病率，分布や形態について後ろ向きに調査した．

結　果：男性1,752例，女性1,261例の合計3,013例（調査時平均年齢65歳）についての調査が可能であった．胸椎OYLは1,094例（36%）［男性666例，女性428例］に認められ，男性に有意に多かった．単椎間罹患は532例，多椎間罹患は562例に認められた．OYLは合計2,051椎間存在し，椎弓の谷に存在するcentral typeが779椎間，non-central type（従来型）が1,272椎間であった．罹患高位は，Th10/Th11にもっとも高いピークと，Th4/Th5に2番目に高いピークとをもつ二峰性分布を示した．年代別分布では，30歳代以降はほぼ一定の罹患率を示した．

結　論：胸部CT検査データからみた日本人の胸椎OYLの有病率は36%であった．椎弓の谷に存在するキノコ型骨化病変もOYLである．臨床症状とOYLのサイズや形態などとの関連が残された研究課題である．

❶ はじめに

黄色靱帯骨化症（ossification of the yellow ligament：OYL）は，Polgar[2)]により1920年にはじめて報告された疾患であり，黄色靱帯が骨組織により置換され脊髄を圧迫することにより脊髄症をきたす．OYLは東アジア人に多く認められると報告されている[3)]が，その疫学については不明な点も多い．OYLの好発部位は胸椎とされているが，肩や肋骨が重なるという解剖学的特徴から，特に上位胸椎においては単純X線像による評価は容易でない．一方，コンピュータ断層撮影（CT）は，解剖学的特徴にかかわらず骨化病変を詳細に描出することが可能な優れたモダリティーである．

われわれは，骨病変の描出に優れるCTを用いて日本人の胸椎OYLの有病率や分布，罹患形態などを調査した[1)]．

❷ 対象および方法

2010年1～9月に胸部疾患，またはその疑いのために当大学を受診し，胸部CT検査が施行された症例のうち，胸椎手術の既往があるもの，15歳以下の症例を除く連続する3,013例（男性1,752，女性1,261）例を対象とした．調査時平均年齢は65歳であった．撮影済みの胸部CTデータをソフトウェア（AquariusNet Viewer：TeraRecon社，Foster City）を用いて骨条件に変換の後，胸椎OYLの有無や分布，罹患形態などを調査した．本ソフトウェアにより任意に冠状断，矢状断，水平断画像を再構築のうえ，連動させて評価が可能であり，骨化病変の詳細な検討が可能となった．CTによるOYLの形態分類には確立されたものがなく，独自

Key words：OYL, thoracic spine, CT, prevalence

* K. Mori（講師）：滋賀医科大学整形外科（Dept. of Orthop. Surg., Shiga University of Medical Science, Otsu）．

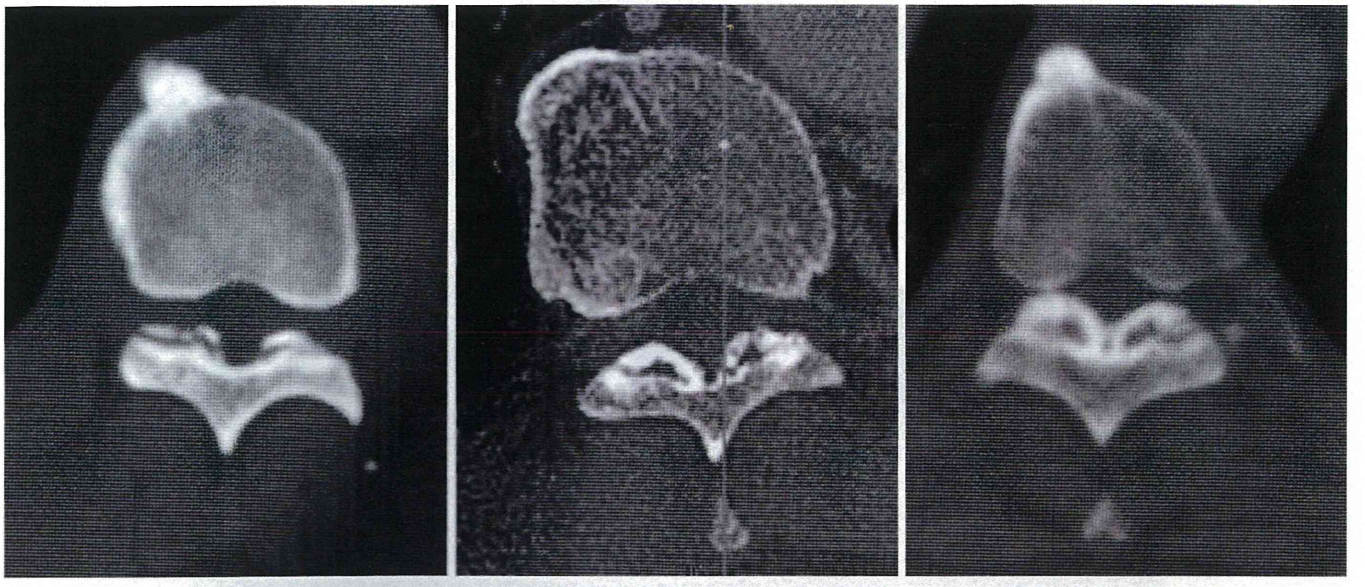

a. Small　　b. Medium　　c. Large

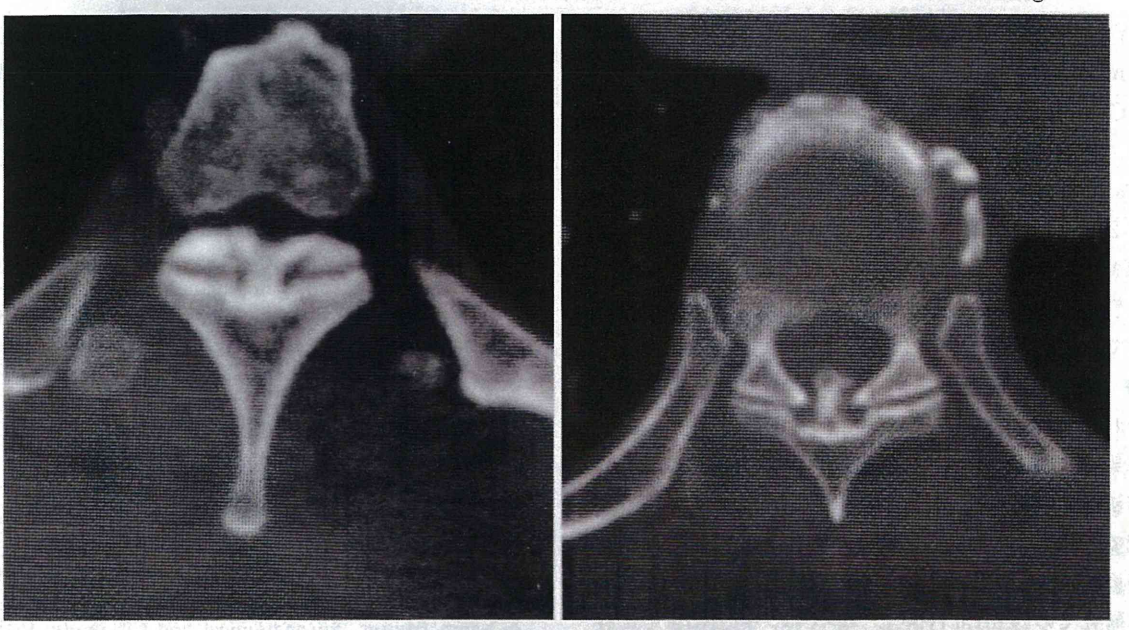

d. Extra large　　e. Central

図 1. CT 水平断における胸椎黄色靱帯骨化症の分類（文献 1 より転載）

に基準を設けた（図 1）．従来型骨化（図 1a～d）のほか，椎弓の谷に存在するキノコ型骨化病変（図 1e）は，当大学での手術時摘出病変の組織学的検討により本病変も OYL であることを確認し，central type とした．また，年齢や body mass index（BMI）などもあわせて調査した．

本研究は，本学の倫理委員会の承認を得て行われた．

❸ 結　　果

本研究において，central type を含めた胸椎 OYL は 1,094 例（36%：男性 666 例，女性 428 例）に認められ，平均年齢は 66（16～93）歳であった．OYL は男性の 38%，女性の 34%に認められ，男性に有意に多かった．男性で OYL を認めた症例は有意に高齢であった（$p<0.0001$）．一方，OYL の有無と女性の年齢や BMI との間には有意な関連を認めなかった．

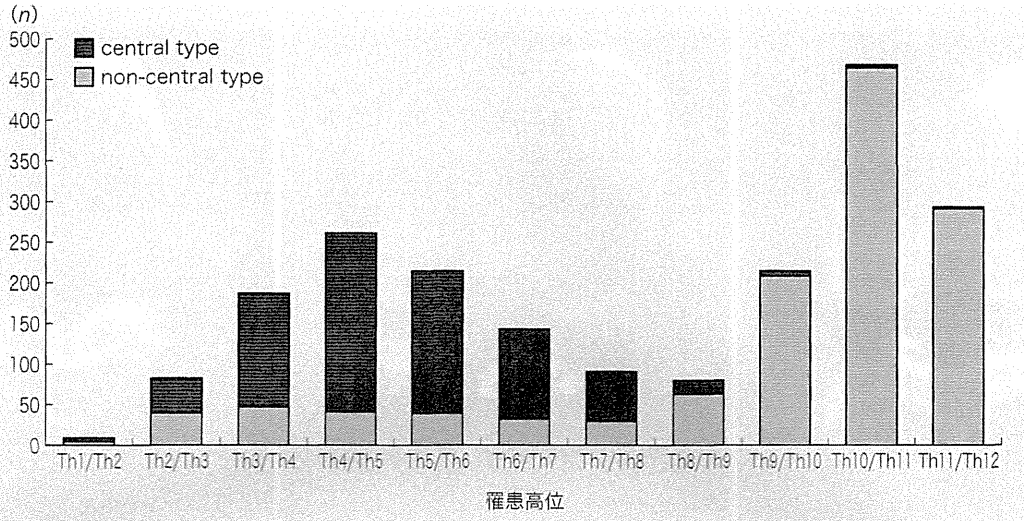

図 2. 胸椎黄色靱帯骨化症の罹患高位分布

OYL の大きさ別では，non-central type は small 37%，medium 40%，large 16%，extralarge 7%であった．Central type は small 26%，medium 46%，large 19%，extralarge 9%であった．単椎間罹患は 532 例（49%），多椎間罹患は 562 例（51%）であり，OYL は合計 2,051 椎間に認められた．罹患高位分布は，もっとも高いピークを Th10/Th11 に，次に高いピークを Th4/Th5 にもつ二峰性分布を示した（図 2）．年代別の検討では，30 歳代以降はほぼ一定の罹患率を示した．

❹ 考　　察

われわれの渉猟した限りでは，OYL の有病率に関する 4 編の英文報告[4-7]があるが，いずれも対象年齢や調査方法などに限界がある．直接比較はむずかしいが，本研究での OYL の有病率は既存の報告と比較して高率であり，CT の高描出力のもたらした結果と考えられる．

本研究での central type については，過去にもその存在が指摘されている[5,8]が，OYL としての分類に言及した詳細な報告は本報告がはじめてである．本研究の限界としては，対象が胸部疾患またはその疑いのある患者であることである．われわれの渉猟しえた限りでは，胸部疾患と脊柱靱帯骨化との関連性を示す報告は見出せなかったが，関連性を完全否定するものではない．一方，本研究の一番の利点は，調査対象者に新たな放射線被曝を課すことなく CT による骨化病変の調査が可能であったことである．

❺ おわりに

胸部 CT からみた日本人胸椎 OYL の有病率は 36%であった．椎弓の谷に存在するキノコ型骨化病変も OYL である．臨床症状と脊柱管占拠率や形態などとの関連についての調査が今後の課題である．

文　献

1) Mori K, Kasahara T, Mimura T et al：Prevalence, distribution, and morphology of thoracic ossification of the yellow ligament in Japanese；results of CT-based cross-sectional study. Spine **38**：E1216-E1222, 2013
2) Polgar F：Uber interakuelle wirbelverkalkung. Fortschr Geb Rongenstr Nuklearmed Erganzungsband **40**：292-298, 1920
3) Yonenobu K, Ebara S, Fujiwara K et al：Thoracic myelopathy secondary to ossification of the spinal ligament. J Neurosurg **66**：511-518, 1987
4) Kudo S, Ono M, Russell WJ. Ossification of thoracic ligament flava. AJR **141**：117-121, 1983
5) Williams DM, Gabrielsen TO, Latack JT et al：Ossification in the cephalic attachment of the ligamentum flavum；an anatomical and CT study. Radiology **150**：423-426, 1984
6) Ohtsuka K, Terayama K, Yanagihara M et al：An epidemiological survey on ossification of ligaments in the cervical and thoracic spine in individuals over 50 years of age. Nihon Seikeigeka Gakkai Zasshi **60**：1087-1098, 1986
7) Guo JJ, Luk KD, Karppinen J, et al：Prevalence, distribution, and morphology of ossification of the ligamentum flavum；a population study of one thousand seven hundred thirty-six magnetic resonance imaging scans. Spine **35**：51-56, 2010
8) 柳　　務，内藤明子，安田武司ほか：黄色靱帯骨化の形態—病理学的所見と CT スキャン像．整形外科 **38**：297-307，1987

Spine

SPINE Volume 39, Number 21, pp E1261-E1268

CERVICAL SPINE

Modified K-line in Magnetic Resonance Imaging Predicts Clinical Outcome in Patients With Nonlordotic Alignment After Laminoplasty for Cervical Spondylotic Myelopathy

Takashi Taniyama, MD,*† Takashi Hirai, MD, PhD,*†‡ Toshitaka Yoshii, MD, PhD,*†
Tsuyoshi Yamada, MD, PhD,*† Hiroaki Yasuda, MD,*† Masanori Saito, MD,*† Hiroyuki Inose, MD, PhD,*
Tsuyoshi Kato, MD, PhD,* Shigenori Kawabata, MD, PhD,* and Atsushi Okawa, MD, PhD*†§

Study Design. Retrospective single-center study.

Objective. To investigate whether a preoperative index predicts clinical outcome after laminoplasty for cervical spondylotic myelopathy.

Summary of Background Data. This is the first study using the modified K-line, which connects the midpoints of the spinal cord at the C2 and C7 levels on midsagittal magnetic resonance imaging, to assess the relationship between postoperative clinical outcome and anticipated degree of spinal cord shifting.

Methods. Sixty-one consecutive patients who underwent laminoplasty for the treatment of cervical spondylotic myelopathy between 2000 and 2011 at our hospital were retrospectively reviewed. The interval between the preoperative mK-line and the anterior structure of the spinal canal at each segment of the C3 to C6 levels (INT_n, n = 3–6) were measured on sagittal T1-weighted magnetic resonance imaging, and the sum of the INT_n (INT_{sum}) was then calculated. The degree of posterior cord shift was defined as follows: $\%C_{sum} = \Sigma C_n$; $C_n = (B_n - A_n) \times 100/A_n$ (n = 3–6; A_n and B_n represent the preoperative and postoperative intervals between the midpoint of the spinal cord and the anterior impingement at each segment on sagittal T1-weighted magnetic resonance imaging, respectively). In addition, we defined INT_{min} as the minimum interval of the INT_n in each patient. All patients were divided into lordotic and nonlordotic groups on the basis of lateral neutral radiography. The Japanese Orthopaedic Association (JOA) scoring system and recovery rate of the JOA score for cervical myelopathy was evaluated as clinical outcomes.

Results. The recovery rate of the JOA score was 48.1%. The lordotic and nonlordotic groups contained 38 and 23 patients, respectively. Linear regression analysis revealed that INT_{min} was significantly correlated with the recovery rate of the patients in the nonlordotic group, whereas INT_{sum} was not associated with recovery of the JOA score.

Conclusion. We identified INT_{min} as a predictive factor for clinical outcomes in patients with nonlordotic alignment after laminoplasty.

Key words: cervical spondylotic myelopathy, laminoplasty, spinal cord anterior clearance, postoperative anterior compression.

Level of Evidence: 4

Spine 2014;39:E1261–E1268

Many reports[1–3] have addressed laminoplasty (LAMP) for the treatment of patients with myelopathy since Oyama and Hattori[4] first described the procedure in 1973. Several modifications have been made, and the procedure has been adopted by many spine surgeons as an effective and relatively safe method to decompress the spinal cord[5] and achieve sufficient stability for multisegmental cervical lesions that cause cervical spondylotic myelopathy (CSM).[6] Many reports have indicated that decompression by LAMP leads to long-lasting neurological recovery.[7,8] However, LAMP occasionally fails to relieve anterior compression of spinal cord caused by cervical kyphosis and/or intervertebral disc bulging,[9–11] which prevents neurological recovery, because the decompression mechanism depends only on the posterior shifting of the spinal cord. Therefore, it is important for spine surgeons to acknowledge this issue and determine risk factors

From the *Department of Orthopaedic and Spinal Surgery, Graduate School, Tokyo Medical and Dental University, Tokyo, Japan; †Section of Regenerative Therapeutics for Spine and Spinal Cord, Graduate School, Tokyo Medical and Dental University, Tokyo, Japan; ‡Division of Oral Biology and Medicine, School of Dentistry, University of California, Los Angeles, Los Angeles, CA; and §Global Center of Excellence (GCOE) Program for International Research Center for Molecular Science in Tooth and Bone Disease, Tokyo Medical and Dental University, Tokyo, Japan.

Acknowledgment date: February 27, 2014. Revision date: May 15, 2014. Acceptance date: July 15, 2014.

The manuscript submitted does not contain information about medical device(s)/drug(s).

No funds were received in support of this work.

No relevant financial activities outside the submitted work.

Address correspondence and reprint requests to Takashi Hirai, MD, PhD, Department of Orthopedic Surgery, Tokyo Medical and Dental University, 1-5-45 Yushima, Bunkyo-Ku, Tokyo 113-8519, Japan; E-mail hirai.orth@tmd.ac.jp or Division of Oral Biology and Medicine, School of Dentistry, University of California, Los Angeles, 10833 Le Conte Ave, Los Angeles, CA 90095; E-mail htakacy@ucla.edu

DOI: 10.1097/BRS.0000000000000531

for ineffective or incomplete decompression before selecting a surgical treatment. We previously reported that the modified K-line (mK-line) in magnetic resonance imaging (MRI) is an effective tool to predict residual anterior compression of the spinal cord after LAMP.[12] In this study, we further investigated whether preoperative factors determined according to the mK-line could predict postoperative spinal cord shifting and clinical outcomes after LAMP in patients with CSM.

MATERIALS AND METHODS

Patients and Methods

We conducted a retrospective, observational, single-center study of posterior decompression with LAMP for the treatment of CSM. The study was conducted with the approval of the Institutional Ethics Committee of Tokyo Medical and Dental University (#1681). Patients with cervical myelopathy caused by spondylosis were included in the study. Exclusion criteria were myelopathy caused by single-level disc herniation or ossification of posterior longitudinal ligament, a history of cervical spine surgery, postoperative epidural hematoma, and cases in which preoperative and postoperative magnetic resonance (MR) images could not be obtained. Patients who had cervical kyphosis in which the sagittal lordotic angle was greater than 13° were not enrolled in this study.[13] Sixty-one consecutive patients in our hospital who underwent LAMP for the treatment of CSM between 2000 and 2011 were reviewed. All patients were followed up for more than 2 years. Patient demographic data are shown in Table 1. The mean patient age was 65.8 years (range: 42–82 yr). The decompression was performed from C3 to C7 in 46 patients, from C3 to C6 in 11 patients, from C4 to C6 in 1 patient, and from C4 to C7 in 3 patients. The mean Japanese Orthopaedic Association (JOA) score before surgery was 8.6 points (range: 3.5–13.5). The mean JOA score at the final visit was 12.5 points (range: 6.5–16.5), yielding a mean recovery rate (RR) of 48.1% (range: 0–94.4). None of these patients presented a worsened neurological outcome after surgery. The average C2–C7 lordotic angle was 14.3° of lordosis (range, 10.8° of kyphosis to 37.1° of lordosis). Cervical alignment was categorized according to criteria defined by Kamata *et al*[14,15] in all patients (Figure 1A). Regarding alignment, 38 patients were lordotic, 7 straight, 5 kyphotic, 8 sigmoid, and 3 reversed-sigmoid. These 61 patients were divided into a lordotic group (n = 38) and a nonlordotic group (n = 23).

TABLE 1. Demographic Data

	Mean ± SD
Age at surgery, yr	65.8 ± 9.8
Sex (M:F)	44:17
No. of patients	
C3–C7	46
C3–C6	11
C4–C6	1
C4–C7	3
Pre-JOA score	8.6 ± 3.0
Post-JOA score	12.5 ± 3.2
JOA recovery rate (%)	48.1 ± 26.8
Preoperative C2–C7 lordotic angle (degrees)	17.6 ± 14.3
Global sagittal alignment	
Lordosis	38
Straight	7
Kyphosis	5
Sigmoid	8
Reversed sigmoid	3

JOA indicates The Japanese Orthopaedic Association.

Operative Technique

Expansive LAMP was performed as described by Miyazaki and Kirita.[16] Briefly, this procedure performed at C3–C7 included removing the C4–C6 processes, splitting the laminae at the center, making bilateral gutters from C3 to C6, and fenestration at the cephalad portion of the lamina of C7 using a high-speed air-burr drill. LAMP at C3–C6 comprised splitting the laminae at C3–C6 without fenestration at the C7 laminae. The laminae were kept open with anchor sutures in the deep fascia, and small bone chips obtained from the spinous processes were inserted into the gap between the laminae and the facets and into the bilateral gutter. Patients were instructed to wear a neck collar for 2 to 4 weeks postoperatively.

Evaluations

Clinical Findings

The JOA scoring system[17] was used to evaluate the severity of cervical myelopathy before and after surgery. The RR was calculated using the method of Hirabayashi *et al*[18] to compare pre- and postoperative JOA scores. The duration of preoperative symptoms was also investigated. The segment responsible for myelopathy was diagnosed on the basis of radiological, electrophysiological, and neurological findings.

Radiological Evaluations

Radiographical studies were conducted in all patients and results were evaluated by 2 independent spine surgeons. MR image was obtained both before and within 3 months after surgery for all patients. All MR images were obtained on a 1.5-Tesla scanner (Signa HDxt 1.5T; GE Healthcare, Waukesha, WI), and the MRI protocol consisted of the following conventional MR sequences: sagittal T1-weighted spin-echo (SE): repetition time (TR)/echo time (TE): 480/9 milliseconds, spacing 3 mm; sagittal T2-weighted SE: TR/TE: 3000/85 milliseconds, spacing 3 mm; transaxial T1-weighted SE: TR/TE: 460/10 milliseconds; and transaxial T2-weighted SE: TR/TE: 4020/110 milliseconds. As we previously reported,[12] the

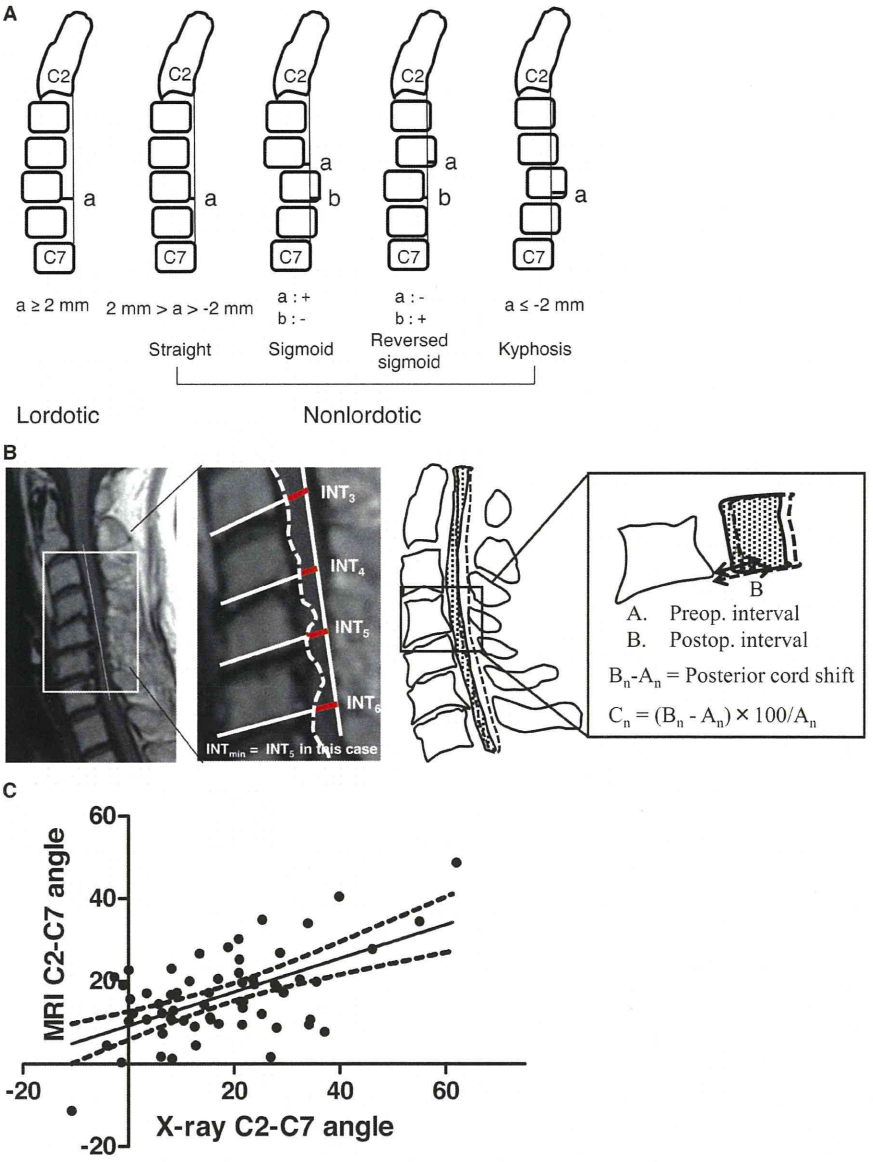

Figure 1. A, Classification of cervical alignment by Kamata *et al.*[14,15] B, The modified K-line (mK-line) was defined as the line connecting the midpoints of the spinal cord at C2 and C7 on preoperative T1-weighted sagittal magnetic resonance imaging (*left*). The interval (INT_n) between the K-line and the most anterior feature of the spinal canal at each segment was measured (n = 3–6; *center*). The minimum interval between the mK-line and the anterior compression-causing feature of the spinal canal in the midsagittal image was defined as INT_{min} (*center*). The interval between the midpoint of the cord and posterior edge of the anterior factor before and after surgery was measured and then the spinal cord shift at each segment was calculated (*right*). C, A significant correlation between the C2–C7 angle on magnetic resonance imaging and that on radiography was observed in this series ($y = 0.407x + 9.275$, y: MRI: C2–C7, x: radiography: C2–C7, $r^2 = 0.332$; $P < 0.01$), suggesting that the neck position at which magnetic resonance imaging was obtained was similar to the cervical neutral position. MRI indicates magnetic resonance imaging. Preop indicates preoperative; Postop, postoperative.

modified K-line was defined as a line connecting the midpoint of the spinal cord at C2 (determined at the level of the inferior endplate) to that at C7 on T1-weighted MR image (mK-line; Figure 1B, *left*). This line is different from the K-line that connects the midpoints of the spinal canal at C2 and C7 on the basis of conventional lateral radiography.[19] The interval (INT_n) between the mK-line and the anterior factor of the spinal canal, such as disc bulging or a bony spur, at each segment (n = 3–6) was measured before surgery. The sum of the measured intervals (INT_{sum}) was then calculated for each patient (Figure 1B, *center*). In addition, INT_{min} was defined as the lowest INT_n in each case, as we previously reported[12] (Figure 1B, *center*), and was also collected for each patient. The pre- and postoperative INT_n at each segment from C3 to C6 were measured on sagittal T1-weighted MR image to evaluate the actual migration of the spinal cord, which was defined as $C_n = (B_n - A_n) \times 100/A_n$ (n = 3–6; A_n and B_n represent the preoperative and postoperative INT_n, respectively, Figure 1B, *right*). To evaluate the global posterior migration of the spinal cord, we calculated $C_{sum} = C_3 + C_4 + C_5 + C_6$ and then analyzed the relationship between preoperative INT_n and C_n (n = 3–6) to determine whether the mK-line could predict a postoperative shift in the spinal cord. The presence of signal intensity changes in the cord was also evaluated on sagittal view T2-weighted MR images of each patient. In preoperative radiography, the cervical sagittal alignment (C2–C7 lordotic angle), determined from tangential lines drawn on the posterior edges of the C2 and C7 bodies, was measured on mid-sagittal MRI and on X-rays obtained in the cervical neutral position to determine whether the neck position

on MRI was similar to the cervical neutral neck position on radiography.

Statistical Analysis

Student unpaired *t* test was used to evaluate the differences in each parameter between the lordotic and nonlordotic groups, except for the RR of the JOA score, INT_{sum}, INT_{min}, and C_{sum}, for which the Mann-Whiney *U* test was used. A cross-correlation analysis was used to evaluate the correlation between INT_n and C_n at each segment. A linear regression analysis was used to investigate whether INT_{sum} was correlated to C_{sum} or the RR of the JOA score. All data are expressed as the mean ± SD. *P* value of less than 0.05 was defined as statistically significant.

RESULTS

Sagittal Cervical Alignment Measured by MRI Significantly Correlates With That Measured by Radiography

Prior to investigation of the relationship between the mK-line determined by MRI and the shift in the spinal cord or clinical outcome, we determined whether the sagittal alignment measured by MRI (MRI, C2–C7) agreed with that measured by neutral radiography (C2–C7) in each case. There was a significant correlation between MRI, C2–C7 and radiography, C2–C7 in this series ($y = 0.407x + 9.275$; *y*: MRI, C2–C7; *x*: radiography, C2–C7; $r^2 = 0.332$; $P < 0.01$, Figure 1C). This result suggests that the neck position at which MR image was obtained was similar to the cervical neutral position.

Anticipated Cord Shift Calculated Using the mK-line Significantly Correlates With Actual Posterior Cord Shift

Table 2 shows the values for INT_n and C_n (Figure 1B, *right*) at each segment in all patients (n = 3–6). The maximum interval was 7.3 mm at the C4 level. The average INT_{sum} value was 27.5 mm. Similarly, the maximum posterior cord shift was 30.3% at the C4 level and the average C_{sum} was 99.3%. Cross-correlation analysis demonstrated significant similarity between the waveform distribution of INT_n and that of C_n ($R = 0.889$, $P < 0.05$; Figure 2A).

INT_{sum} Predicts the Posterior Shift of the Spinal Cord in Lordotic But Not in Nonlordotic Patients

There were no significant differences in age, ratio of males, preoperative JOA score, RR of JOA score, posterior shift of the whole spinal cord, positive ratio of the presence of signal intensity changes in the spinal cord, or incidence of C5 palsy between the lordotic and nonlordotic groups (Table 3). However, we found that patients in the lordotic group had a higher preoperative lordosis angle, INT_{sum}, and INT_{min} than patients in the nonlordotic group (Table 3). In addition, INT_{sum} was associated with $\%C_{sum}$ only in the lordotic group ($y = 4.527x - 36.48$, $y = \%C_{sum}$, $x = INT_{sum}$, $r^2 = 0.1333$, $P < 0.05$; Figure 2B); there was no significant correlation between INT_{sum} and C_{sum} in the nonlordotic group (data not shown).

TABLE 2. Interval Between the K-line and the Anterior Feature of the Spinal Canal and the Extent of Actual Posterior Cord Migration at Each Segment*

Segment	Interval (mm)	Ratio of Posterior Cord Shift (C_n)
C3	6.5 ± 2.6	17.9 ± 26.8
C4	7.3 ± 3.1	30.3 ± 31.5
C5	6.9 ± 2.7	28.9 ± 33.9
C6	6.8 ± 2.2	22.2 ± 31.6
Total	INT_{sum} = 27.5 ± 9.0	C_{sum} = 99.3 ± 83.7

**Data are expressed as the mean ± SD.*

INT_{sum} indicates the sum of the intervals between the K-line and the anterior feature of the spinal canal at each segment (C3–C6); C_n: $(B_n - A_n) \times 100/A_n$ (n = 3–6; A_n and B_n represent the preoperative and postoperative intervals between the midpoint of the spinal cord and the anterior impingement at each segment from C3 to C6 levels); C_{sum}, the sum of C3, C4, C5, and C6.

INT_{sum} Is Not a Predictive Factor for Postoperative Clinical Outcome After LAMP

To evaluate the relationship between anticipated postoperative cord shift determined from preoperative MRI and clinical outcomes, we analyzed a linear regression model for INT_{sum} and the RR of the JOA score in each group. The linear regression analysis indicated no significant correlation between INT_{sum} and the RR of the JOA score in both groups (data not shown).

INT_{min} Can Predict Clinical Outcome in Nonlordotic Patients

It is important for spine surgeons to predict postoperative clinical outcomes, particularly in patients with cervical misalignment such as kyphotic or sigmoid alignment, before selecting a surgical procedure for the treatment of CSM. As several studies have reported,[20–23] age, duration of symptoms, and the presence of signal intensity changes in the spinal cord observed on T2-weighted sagittal MR image are risk factors for poor outcome after surgical treatment. Although we did not find significant associations between clinical outcome and either age or duration of preoperative symptoms using linear regression models, we observed that the RR in patients older than 75 years was poorer than that in younger patients in both groups (data not shown). In addition, because most of the patients presented high signal intensity changes in the spinal cord on T2-weighted imaging in both the lordotic and nonlordotic groups, we were not able to analyze whether the signal intensity change in the spinal cord was associated with poor clinical outcome in this series.

Next, we focused on INT_{min}, which has been shown to be a powerful tool to predict residual anterior impingement of the spinal cord after LAMP,[12] for potential prediction of postoperative neurological outcome in nonlordotic patients. Although INT_{min} was not associated with the RR of the JOA score in lordotic patients (data not shown), it was significantly

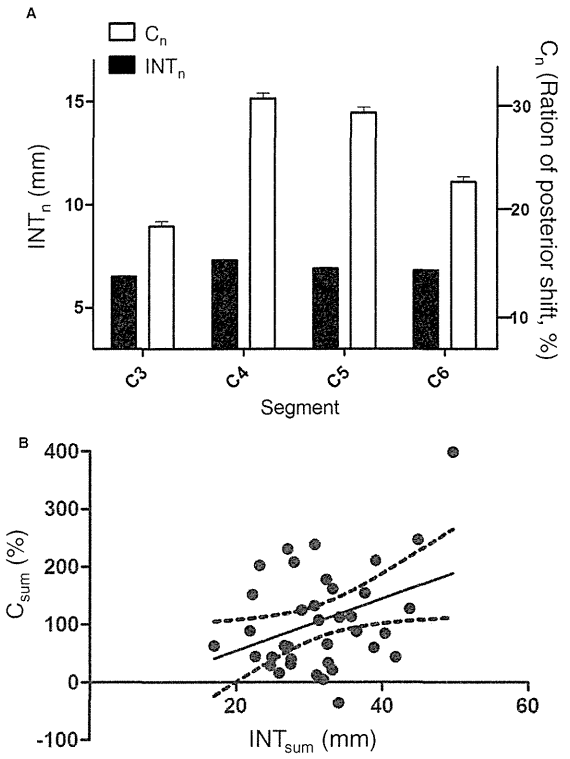

Figure 2. A, The maximum interval was 7.3 mm at the C4 level, and the maximum posterior cord shift was 30.3% at the C4 level. Cross-correlation analysis demonstrated significant similarity between the waveform distribution of INT_n and that of C_n ($R = 0.889$, $P < 0.05$). B, INT_{sum} was significantly correlated with C_{sum} in only the lordotic patient group ($y = 4.527x - 36.48$, $y = C_{sum}$, $x = INT_{sum}$, $r^2 = 0.1333$; $P < 0.05$).

and positively correlated with the RR in nonlordotic patients ($y = 6.347x + 22.36$, y = JOA score RR, $x = INT_{min}$, $r^2 = 0.2491$, $P < 0.05$; Figure 3). Based on this analysis, an RR higher than 50% requires INT_{min} of greater than 4.4 mm in nonlordotic patients.

Case Presentation

A 68-year-old male presented with bilateral hand numbness and clumsiness. Preoperative sagittal MR image showed that an anterior feature at the C3–C4 level was related to local kyphosis on sigmoid alignment (Figure 4, *left*). Although he received LAMP for multisegmental stenosis, postoperative compression of the dural sac and anterior spinal cord existed at the C3–C4 level on MR image (Figure 4, *right*). Although INT_{sum} was 22.2 mm, which was higher than the average value in the nonlordotic group, the preoperative INT_{min} was 1.7 mm at the C3–C4 level. The JOA score recovered by 33.3% and the persistent numbness of both upper extremities remained even after surgery; therefore, an anterior procedure or posterior decompression with corrective fusion should have been applied in this case.

DISCUSSION

LAMP has been reported to be effective, relatively low cost, minimally invasive, and safe for the treatment of patients with

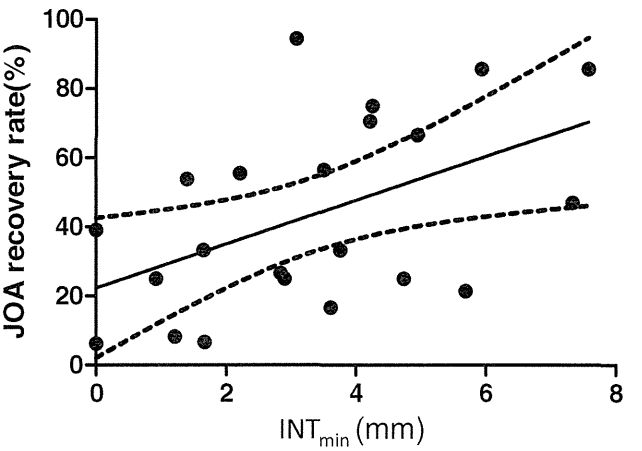

Figure 3. A significant positive correlation between INT_{min} and the recovery rate of the JOA score was confirmed ($y = 6.347x + 22.36$, y = JOA score recovery rate, $x = INT_{min}$, $r^2 = 0.2491$; $P < 0.05$). JOA indicates The Japanese Orthopaedic Association.

multilevel spondylosis or ossification of the posterior longitudinal ligament.[5–8,24] However, undesirable outcomes after LAMP can be caused by residual anterior compression of the spinal cord resulting from preoperative cervical misalignment and progression of kyphosis or loss of lordosis. The resulting pathology often reduces the quality of life and may require secondary surgery. Therefore, it is necessary to determine the factors that limit the efficacy of posterior decompression. In the current study, we optimized new indices, INT_{sum} and INT_{min}, on the basis of the mK-line and evaluated whether they could be useful for surgical treatment decisions.

We found that the interval between the mK-line and the anterior feature of the spinal column, that is, INT_n on preoperative MRI, was closely associated with the actual posterior cord shift at each vertebral level after LAMP. Furthermore, we showed that both INT_{sum} and INT_{min} were significantly higher in the lordotic group than in the nonlordotic group. These findings are consistent with the frequent observation of anterior clearance of the spinal cord in patients with a lack of cervical lordosis, thereby suggesting that the mK-line may be useful to evaluate impingement of the spinal cord by the anterior feature of the spinal column.

Furthermore, we quantified the posterior shift of the whole spinal cord as INT_{sum} for prediction of postoperative clinical outcome. Baba *et al*[23] previously showed that the magnitude of posterior cord migration after LAMP was significantly correlated with postoperative neurological outcome. In the current study, the anticipated cord migration, defined as INT_{sum}, was not associated with the RR of the JOA score. However, because patients with INT_{sum} of 20 mm or greater tended to achieve better outcomes than patients with INT_{sum} of less than 20 mm, INT_{sum} may be useful for prediction of clinical and radiological outcomes.

We also investigated the relationship between the segment responsible for the myelopathy and the level at which INT_{min} was measured. Indeed, the level at which INT_{min} was observed did not always correspond to the segment responsible for the

TABLE 3. Demographic Data for Each Group*

	Lordotic Group (n = 38)	Nonlordotic Group (n = 23)	*P*
Age, yr	67.8 ± 9.0	67.7 ± 11.0	ND
Male (%)	65.8%	82.6%	ND
Duration of symptoms, mo	11.8 ± 12.5	13.9 ± 10.9	ND
Preoperative JOA score	8.2 ± 3.2	8.5 ± 3.3	ND
Postoperative JOA score	12.5 ± 3.5	12.0 ± 2.9	ND
Recovery rate of the JOA score	51.6 ± 26.6	42.2 ± 27.4	ND
Preoperative C2–C7 lordotic angle (degrees)	25.1 ± 12.1	5.2 ± 8.0	<0.01
INT_{sum}	31.5± 7.1	20.8 ± 8.1	<0.01
INT_{min}	6.27 ± 1.9	3.38 ± 2.1	<0.01
Posterior shift of the whole spinal cord (C_{sum})	113.3 ± 95.8	77.2 ± 56.6	ND
Positive ratio of signal intensity change in the spinal cord (%)	94.7	82.6	ND
Segment responsible (cases)			
C3–C4	10	5	ND
C4–C5	12	8	ND
C5–C6	16	9	ND
C6–C7	0	1	ND
Incidence of C5 palsy	2 cases/5.3%	2 cases/8.7%	ND

**Data are expressed as the mean ± SD.*

ND indicates no significant difference; JOA, The Japanese Orthopaedic Association; INT_{sum}, sum of the intervals between the K-line and the anterior element of the spinal canal at each segment (C3–C6); INT_{min}, the minimum interval between the preoperative modified K-line and the anterior impingement on midsagittal imaging; C_n, $(B_n - A_n) \times 100/A_n$ (n = 3–6; A_n and B_n, represent the preoperative and postoperative intervals between the midpoint of the spinal cord and the anterior impingement at each segment from C3 to C6 levels); C_{sum}, sum of C3, C4, C5, and C6.

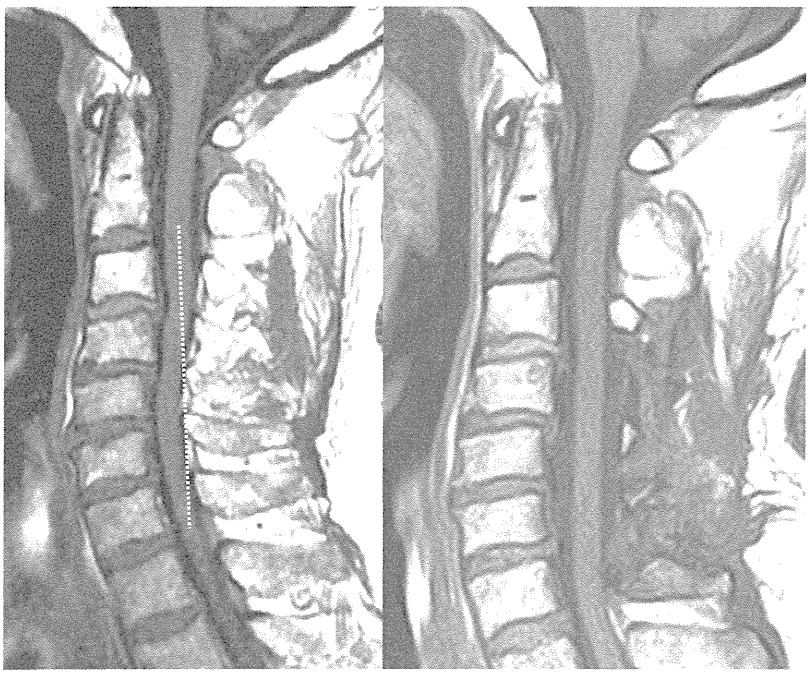

Figure 4. Preoperative magnetic resonance imaging shows that anterior compression at the C3–C4 level is caused by local kyphosis on sigmoid alignment. In this case, INT_{sum} and INT_{min} were 22.2 mm and 1.7 mm, respectively (*left*). Postoperative magnetic resonance imaging demonstrates that anterior compression of the dural sac and anterior spinal cord remained at the C3–C4 level even after posterior decompression (*right*).

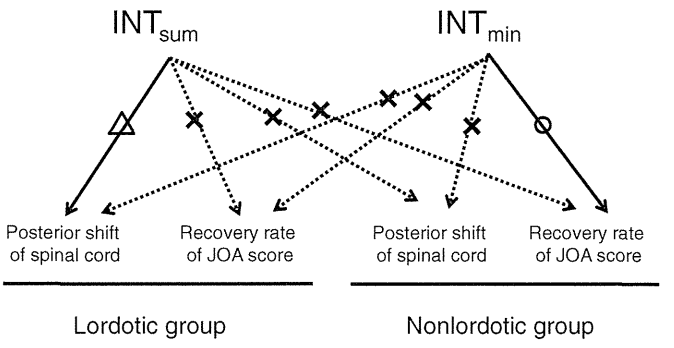

Figure 5. Summary of this study. Although INT_{sum} was associated with the magnitude of posterior cord shifting after laminoplasty in patients with lordotic alignment, it was not a predictive factor for postoperative clinical outcome. In contrast, INT_{min} was significantly correlated with postoperative neurological improvement in patients with nonlordotic alignment, whereas there was no association between INT_{min} and the degree of posterior cord shifting. JOA indicates The Japanese Orthopaedic Association.

myelopathy diagnosed by electrophysiology; in 10 patients, the segment responsible for myelopathy was typically C4–C5 or C5–C6, whereas the level with the highest compression was C3–C4 or C6–C7. Two of these 10 patients could not obtain sufficient cord migration at the C3–C4 level and thus obtained unsatisfactory outcomes. In such cases, it is still important to pay attention to the level with the highest compression, although it is not diagnosed as the causative segment by electrophysiologic and neurological findings, because residual cord compression in the noncausative segment still contributes to the myelopathic symptomatology and is thus a risk factor for myelopathic deterioration after LAMP.

In addition, we also investigated whether the anticipated cord migration could predict the onset of C5 palsy, which is a major complication after LAMP[25] and for which excessive posterior cord shift has been considered as a possible cause. However, we did not observe a significant association between the degree of posterior cord shifting and the incidence of C5 palsy. Previous reports have suggested various other causes for C5 palsy after LAMP, including (1) nerve root traction caused by posterior spinal cord shifting,[26] (2) anatomical stenosis of the C5 foramen,[27] (3) spinal cord ischemia caused by decreased blood supply from radicular arteries,[28] (4) laminar width of decompression,[29] and (5) segmental spinal cord disorder.[25,30] These factors may contribute to the onset of postoperative C5 palsy in a complex manner, and it may, therefore, not be possible to predict the C5 palsy by only measuring the anticipated cord shift.

The relationship between cervical kyphotic alignment and postoperative clinical outcomes after LAMP is controversial. Suda *et al*[13] reported that LAMP is not effective for patients with global kyphosis greater than 13° and no signal change on T2-weighted MR image. Uchida *et al*[31] suggested that correction of local sagittal alignment should be attempted in patients with kyphotic deformity greater than 10° to maximize neurological improvement. Thus, because excessive kyphotic alignment has been recognized as a risk factor for poor outcomes after posterior decompression over the last decade, many studies have recommended that anterior decompression or posterior decompression with fusion should be applied to such misalignment cases.[5,13,31]

However, Kaptain *et al*[32] investigated 46 patients with CSM and concluded that clinical outcome does not usually correlate with preoperative sagittal alignment. This report is consistent with mounting evidence that neurological improvement is influenced by not only global kyphosis but also anterior compression of the spinal cord, which seems to lead to a lack of decompression at the ventral aspect of the spinal cord.[5,11,13,23] Given these 2 morphological factors, it is important to evaluate the physical relationship between the spinal cord and the anterior impingement that may be causing the compression prior to surgical treatment. In addition, spine surgeons should predict postoperative clinical outcomes before selecting a surgical procedure for the treatment of CSM particularly in patients with cervical misalignment. This study demonstrated that neurological improvement after LAMP in patients with nonlordotic alignment was significantly correlated with INT_{min} but not with INT_{sum} (Figure 5). Therefore, neurological improvement in patients with misalignment may require a sufficient posterior cord shift at only the most compressed segment rather than throughout the entire spinal cord.

The limitations of this study include its retrospective nature and relatively small cohort size. In the present study, we divided the patients into only 2 groups and showed that INT_{min} significantly predicted postoperative outcome; however, it may be possible to categorize a larger patient pool into 5 different alignments to determine the relationship between our new index and clinical outcomes in each alignment type. With regard to neck position, although our patients were instructed to maintain a neutral position, this was not usually possible during MRI; however, because all patients followed the same radiographical protocol and alignment on MRI was significantly correlated with alignment measured by neutral radiography, the lack of neutral position does not affect the findings of this study. We, therefore, suggest that INT_{min} can help spine surgeons to decide whether LAMP should be performed in patients with nonlordotic alignment.

➢ Key Points

- ❑ Patients who underwent LAMP for the treatment of CSM were divided into lordosis and nonlordosis groups, and we investigated whether anterior clearance of the spinal cord measured on mK-line plays role for predictive factors of postoperative spinal cord migration and clinical outcome in this study.

- Anterior clearance of global spinal cord (INT_{sum}) tends to be associated with the posterior shift of the spinal cord in patients with lordotic alignment but not in patients with nonlordotic alignment.
- INT_{sum} was not associated with clinical outcome in either lordosis group or nonlordosis group.
- A linear regression analysis showed that anticipated anterior clearance at the most compressive segment (INT_{min}) was a significant predictive factor for postoperative clinical outcome in patients with nonlordotic alignment.

Acknowledgments

Drs. Takashi Taniyama and Takashi Hirai contributed equally to this work.

References

1. Hirabayashi K, Watanabe K, Wakano K, et al. Expansive open-door laminoplasty for cervical spinal stenotic myelopathy. *Spine (Phila Pa 1976)* 1983;8:693–9.
2. Kawai S, Sunago K, Doi K, et al. Cervical laminoplasty (Hattori's method). Procedure and follow-up results. *Spine (Phila Pa 1976)* 1988;13:1245–50.
3. Tsuji H. Laminoplasty for patients with compressive myelopathy due to so-called spinal canal stenosis in cervical and thoracic regions. *Spine (Phila Pa 1976)* 1982;7:28–34.
4. Oyama M, Hattori S. A new method of posterior decompression [in Japanese]. *Central Jpn J Orthop Traumatic Surg.* 1973;16:792–4.
5. Hirai T, Okawa A, Arai Y, et al. Middle-term results of a prospective comparative study of anterior decompression with fusion and posterior decompression with laminoplasty for the treatment of cervical spondylotic myelopathy. *Spine (Phila Pa 1976)* 2011;36:1940–7.
6. Subramaniam V, Chamberlain RH, Theodore N, et al. Biomechanical effects of laminoplasty versus laminectomy: stenosis and stability. *Spine (Phila Pa 1976)* 2009;34:E573–8.
7. Seichi A, Takeshita K, Ohishi I, et al. Long-term results of double-door laminoplasty for cervical stenotic myelopathy. *Spine (Phila Pa 1976)* 2001;26:479–87.
8. Chiba K, Ogawa Y, Ishii K, et al. Long-term results of expansive open-door laminoplasty for cervical myelopathy—average 14-year follow-up study. *Spine (Phila Pa 1976)* 2006;31:2998–3005.
9. Tani T, Ushida T, Ishida K, et al. Relative safety of anterior microsurgical decompression versus laminoplasty for cervical myelopathy with a massive ossified posterior longitudinal ligament. *Spine (Phila Pa 1976)* 2002;27:2491–8.
10. Iwasaki M, Okuda S, Miyauchi A, et al. Surgical strategy for cervical myelopathy due to ossification of the posterior longitudinal ligament. Part 1: clinical results and limitations of laminoplasty. *Spine (Phila Pa 1976)* 2007;32:647–53.
11. Hirai T, Kawabata S, Enomoto M, et al. Presence of anterior compression of the spinal cord after laminoplasty inhibits upper extremity motor recovery in patients with cervical spondylotic myelopathy. *Spine (Phila Pa 1976)* 2012;37:377–84.
12. Taniyama T, Hirai T, Yamada T, et al. Modified K-line in magnetic resonance imaging predicts insufficient decompression of cervical laminoplasty. *Spine (Phila Pa 1976)* 2013;38:496–501.
13. Suda K, Abumi K, Ito M, et al. Local kyphosis reduces surgical outcomes of expansive open-door laminoplasty for cervical spondylotic myelopathy. *Spine (Phila Pa 1976)* 2003;28:1258–62.
14. Kamata M, Hirabayashi K, Satomi K, et al. Postoperative spinal deformity by posterior decompression for cervical spondylotic myelopathy [in Japanese]. *East Jpn J Clin Orthop* 1990;2:86–9.
15. Matsumoto M, Fujimura Y, Suzuki N, et al. Cervical curvature in acute whiplash injuries: prospective comparative study with asymptomatic subjects. *Injury.* 1998;29:775–8.
16. Miyazaki K, Kirita Y. Extensive simultaneous multisegment laminectomy for myelopathy due to the ossification of the posterior longitudinal ligament in the cervical region. *Spine (Phila Pa 1976)* 1986;11:531–42.
17. The Japanese Orthopaedic Association. Criteria for the evaluation of treatment of cervical myelopathy. *J Jpn Orthop Assoc (Tokyo)* 1976;49:Addenda No 12.
18. Hirabayashi K, Miyakawa J, Satomi K, et al. Operative results and postoperative progression of ossification among patients with ossification of cervical posterior longitudinal ligament. *Spine (Phila Pa 1976)* 1981;6:354–64.
19. Fujiyoshi T, Yamazaki M, Kawabe J, et al. A new concept for making decisions regarding the surgical approach for cervical ossification of the posterior longitudinal ligament: the K-line. *Spine (Phila Pa 1976)* 2008;33:E990–3.
20. Yamazaki A, Homma T, Uchiyama S, et al. Morphologic limitations of posterior decompression by midsagittal splitting method for myelopathy caused by ossification of the posterior longitudinal ligament in the cervical spine. *Spine (Phila Pa 1976)* 1999;24:32–4.
21. Yonenobu K, Okada K, Fuji T, et al. Causes of neurologic deterioration following surgical treatment of cervical myelopathy. *Spine (Phila Pa 1976)* 1986;11:818–23.
22. Morio Y, Yamamoto K, Kuranobu K, et al. Does increased signal intensity of the spinal cord on MR images due to cervical myelopathy predict prognosis? *Arch Orthop Trauma Surg* 1994;113:254–9.
23. Baba H, Uchida K, Maezawa Y, et al. Lordotic alignment and posterior migration of the spinal cord following en bloc open-door laminoplasty for cervical myelopathy: a magnetic resonance imaging study. *J Neurol* 1996;243:626–32.
24. Sakai K, Okawa A, Takahashi M, et al. Five-year follow-up evaluation of surgical treatment for cervical myelopathy caused by ossification of the posterior longitudinal ligament: a prospective comparative study of anterior decompression and fusion with floating method versus laminoplasty. *Spine (Phila Pa 1976)* 2012;37:367–76.
25. Sakaura H, Hosono N, Mukai Y, et al. C5 palsy after decompression surgery for cervical myelopathy: review of the literature. *Spine (Phila Pa 1976)* 2003;28:2447–51.
26. Satomi K, Nishu Y, Kohno T, et al. Long-term follow-up studies of open-door expansive laminoplasty for cervical stenotic myelopathy. *Spine (Phila Pa 1976)* 1994;19:507–10.
27. Shinomiya K, Okawa A, Nakao K, et al. Morphology of C5 ventral nerve rootlets as part of dissociated motor loss of deltoid muscle. *Spine (Phila Pa 1976)* 1994;19:2501–4.
28. Komagata M, Nishiyama M, EndohK, et al. Clinical study of the postoperative C5 palsy after cervical expansive laminoplasty; efficacy of bilateral partial foraminotomy for the prevention the C5 palsy [in Japanese]. *J Jpn Spine Res Soc* 2002;131:237.
29. Lubelski D, Derakhshan A, Nowacki AS, et al. Predicting C5 palsy via the use of preoperative anatomic measurements. *Spine J* 2014;14:1895–901.
30. Ohkubo H, Komori H, Ohkawa A, et al. An investigation of the postoperative C5 palsy [in Japanese]. *J Jpn Spine Res Soc* 2002;13:354.
31. Uchida K, Nakajima H, Sato R, et al. Cervical spondylotic myelopathy associated with kyphosis or sagittal sigmoid alignment: outcome after anterior or posterior decompression. *J Neurosurg Spine* 2009;11:521–8.
32. Kaptain GJ, Simmons NE, Replogle RE, et al. Incidence and outcome of kyphotic deformity following laminectomy for cervical spondylotic myelopathy. *J Neurosurg* 2000;93:199–204.

Bone 67 (2014) 208–221

Contents lists available at ScienceDirect

Bone

journal homepage: www.elsevier.com/locate/bone

Original Full Length Article

The temporal and spatial development of vascularity in a healing displaced fracture

Masato Yuasa [a,f,1], Nicholas A. Mignemi [a,b,1], Joey V. Barnett [c], Justin M.M. Cates [b], Jeffry S. Nyman [a,d], Atsushi Okawa [f], Toshitaka Yoshii [f], Herbert S. Schwartz [a,b], Christopher M. Stutz [a], Jonathan G. Schoenecker [a,b,c,d,e,*]

[a] Vanderbilt University Medical Center, Department of Orthopaedics, 2200 Children's Way, Nashville, TN 37232-9565, USA
[b] Vanderbilt University Medical Center, Department of Pathology, C-2314 Medical Center North, Nashville, TN 37232-2561, USA
[c] Vanderbilt University Medical Center, Department of Pharmacology, 438 Robinson Research Building, Nashville, TN 37232-6600, USA
[d] Vanderbilt University Medical Center, Center for Bone Biology, 1255 MRB IV, Nashville, TN 37232-9565, USA
[e] Vanderbilt University Medical Center, Department of Pediatrics, 2200 Children's Way, Nashville, TN 37232-9565, USA
[f] Tokyo Medical and Dental University, Department of Orthopaedic and Spinal Surgery, 1-5-45 Yushima, Bunkyo-ku, Tokyo 113-8510, Japan

ARTICLE INFO

Article history:
Received 17 January 2014
Revised 4 June 2014
Accepted 1 July 2014
Available online 10 July 2014

Edited by: Regis O'Keefe

Keywords:
Bone vascularity
Fracture healing
Angiogenesis
Angiography
Vascular endothelial growth factor
Non-union

ABSTRACT

Underlying vascular disease is an important pathophysiologic factor shared among many co-morbid conditions associated with poor fracture healing, such as diabetes, obesity, and age. Determining the temporal and spatial patterns of revascularization following a fracture is essential for devising therapeutic strategies to augment this critical reparative process. Seminal studies conducted in the last century have investigated the pattern of vascularity in bone following a fracture. The consensus model culminating from these classical studies depicts a combination of angiogenesis emanating from both the intact intramedullary and periosteal vasculature. Subsequent to the plethora of experimental fracture angiography in the early to mid-20th century there has been a paucity of reports describing the pattern of revascularization of a healing fracture. Consequently the classical model of revascularization of a displaced fracture has remained largely unchanged. Here, we have overcome the limitations of animal fracture models performed in the above described classical studies by combining novel techniques of bone angiography and a reproducible murine femur fracture model to demonstrate for the first time the complete temporal and spatial pattern of revascularization in a displaced/stabilized fracture. These studies were designed specifically to i) validate the classical model of fracture revascularization of a displaced/stabilized fracture, ii) assess the association between intramedullary and periosteal angiogenesis and iii) elucidate the expression of VEGF/VEGF-R in relation to the classical model. From the studies, in conjunction with classic studies of angiogenesis during fracture repair, we propose a novel model (see abstract graphic) that defines the process of bone revascularization subsequent to injury to guide future approaches to enhance fracture healing. This new model validates and advances the classical model by providing evidence that during the process of revascularization of a displaced fracture 1) periosteal angiogenesis occurs in direct communication with the remaining intact intramedullary vasculature as a result of a vascular shunt and 2) vascular union occurs through an intricate interplay between intramembranous and endochondral VEGF/VEGF-R mediated angiogenesis.

Introduction

Fracture is arguably the most common medical condition treated by orthopedic surgeons, with over 5 million fractures treated annually in the United States alone [1]. Between 2.5 and 10% of these fracture cases are complicated by delayed union or non-union [2–8]. The increasing incidence of comorbid conditions commonly associated with non-union, such as obesity, diabetes, and age suggests that the rate of non-union will only continue to rise [9–13]. In addition to substantial morbidity for patients, these complications impose a significant cost burden on the health care system. Thus, there are considerable ongoing efforts to develop novel methods of fracture fixation and/or application of bone-inducing biological agents to stimulate fracture healing. Given that angiogenesis is a requisite for fracture healing [14–19] and that vascular dysfunction is common to many comorbid conditions associated with poor fracture healing [20–24], it has been hypothesized that a primary cause of delayed union or non-union is

* Corresponding author at: Vanderbilt University Medical Center, Department of Orthopaedics, 2200 Children's Way, Nashville, TN 37232-9565, USA.
E-mail address: Jon.Schoenecker@vanderbilt.edu (J.G. Schoenecker).
[1] These authors contributed equally on this publication.

http://dx.doi.org/10.1016/j.bone.2014.07.002
8756-3282/

impaired angiogenesis. A necessary step in developing approaches to augment angiogenesis during fracture repair is the identification of the temporal and spatial patterns of vascularization following an injury.

Seminal studies conducted in the last century have investigated the pattern of vascularity in bone following a fracture. Investigations by Kolodny [25], Teneff [26] and Göthman [27] suggest a model in which the dominant source of fracture revascularization is the periosteum and other extra-osseous vascular sources such as adjacent skeletal muscle. Conversely, Ladanyi and Trueta discovered patterns of revascularization that apparently contradicted this model by demonstrating the essential nature of the intramedullary vasculature in revascularization of a fracture [28,29]. In a series of papers published in the 1960s, this controversy was revisited by Rhinelander who showed that the mechanism of revascularization was dependent on the type of experimental fracture model employed [30,31]. He made a key observation that in non-displaced fractures, the intramedullary vascularity reunited relatively early, without development of a significant periosteal component (so-called primary bone healing through "trans-medullary revascularization"). However, a different pattern of revascularization was observed in fractures with significant displacement, even with subsequent reduction and stabilization. In the displaced fracture model, initial formation of new periosteal vasculature was followed by intramedullary revascularization (so-called secondary bone healing or "trans-periosteal revascularization"). Thus, Rhinelander's work resolved the apparent discrepancy by showing that different mechanisms of revascularization are employed in different experimental models (displaced vs. non-displaced fractures). The consensus model of revascularization of a displaced fracture culminating from these classical studies depicts a combination of angiogenesis emanating from both the intact intramedullary and periosteal vasculature.

Subsequent to the plethora of experimental fracture angiography in the early to mid-20th century there has been a paucity of reports describing the pattern of revascularization of a healing fracture. Consequently the classical model of revascularization of a displaced fracture has remained largely unchanged. Determination of the molecular elements responsible for and the pattern of revascularization following a fracture are essential for targeting and augmenting discrete events during fracture healing. Importantly, key elements of fracture revascularization were unclear following the development of this model. Specifically, the association of angiogenesis in the intramedullary and periosteal space was unknown. It was hypothesized, that fracture angiogenesis in these anatomically distinct compartments occurred independently and only formed an anastomosis in the later stages of fracture healing [31]. It was proposed that intramedullary angiogenesis occurred as a result of direct vascular growth from the remaining intact intramedullary vascularity and periosteal angiogenesis occurred as a result of direct vascular growth from the surrounding musculature. Additionally, the factors directing vascular union were unknown as vascular endothelial growth factor (VEGF) and its receptors (VEGF-R) had yet to be discovered [32]. Thus, the molecular patterning leading to vascular union has not been incorporated into this classical model. In addition to these unanswered questions, the principle reason for the lack of advancement in this field has been critical methodological restraints prohibiting high throughput animal studies on fracture vascularity. Specifically, the classical models were performed primarily in relatively cost-inefficient larger animal models without the benefit of axial imaging allowing for detailed evaluation of fracture related angiogenesis.

Here, we have overcome the limitations of animal fracture models performed in the above described classical studies by combining novel techniques of bone angiography and a reproducible murine femur fracture model to demonstrate for the first time the complete temporal and spatial pattern of revascularization in a displaced/stabilized fracture. These studies were designed specifically to i) validate the classical model of fracture revascularization of a displaced/stabilized fracture, ii) assess the association between intramedullary and periosteal angiogenesis and iii) elucidate the expression of VEGF/VEGF-R in relation to the classical model.

From the studies, in conjunction with classic studies of angiogenesis during fracture repair [25,26,28,30,31,33–43], we propose a novel model (see abstract graphic) that defines the process of bone revascularization subsequent to injury to guide future approaches to enhance fracture healing. This new model validates and advances the classical model by providing evidence that during the process of revascularization of a displaced fracture 1) periosteal angiogenesis occurs in direct communication with the remaining intact intramedullary vasculature as a result of a vascular shunt and 2) vascular union occurs through an intricate interplay between intramembranous and endochondral VEGF/VEGF-R mediated angiogenesis.

Materials & methods

Murine fracture model and X-ray imaging

Protocols were approved by the Vanderbilt University IACUC. Open femur osteotomies were performed and fixed as previously described using a medial approach to the mid-shaft femur of 8 week old c57/b6 mice. The fracture was fixed through the placement of a 23-G (0.6414 mm) retrograde intramedullary pin and the mice were examined from 7 to 42 days after fracture [44]. X-ray was performed as previously described [45]. Briefly, the mice were placed in the prone position and imaged for 4 s at 45 kV using a Faxitron LX 60. The mice were sacrificed at various time points (7–42 days) following a fracture.

Angiography

Perfusion with Microfil (MV-122 Flow Tech Inc., Carver, MA) vascular contrast was conducted as previously described [46–49]. Briefly, the mice were euthanized, positioned supine and a thoracotomy extending into a laparotomy was performed. The left ventricle of the heart was cannulated using a 25-G butterfly needle. The inferior vena cava (IVC) was transected proximal to the liver and the entire vasculature subsequently perfused with 9 ml of warm heparinized saline (100 units/ml in 0.9% saline) through the left ventricle cannula to exsanguinate and anticoagulate thus preventing erythrocyte aggregation and thrombosis thereby promoting consistent perfusion of subsequent infusion materials. Exsanguination and anticoagulation was deemed complete upon widespread hepatic blanching with clear fluid extravasating from the IVC. The mice were then perfused with 9 ml of 10% neutral buffered formalin followed by 3 ml of Microfil (Flow Tech inc. Carver Massachusetts) vascular contrast polymer. To best verify complete filling of the vasculature gross images of the liver (Supplemental Fig. 1a), the last organ to be perfused prior to extravasation through the IVC, was examined for extravascular pooling. The mice were excluded from the study if complete hepatic blanching prior to Microfil was not achieved, if contrast was not clearly or uniformly visible in the hepatic vasculature or if extravascular pooling occurred. Inspection of hepatic perfusion revealed no differences between manual and infusion pump perfusion set at a constant rate of 0.5 ml/min (Supplemental Fig. 2a). Manual filling was conducted at a goal rate approximately equal to the pump rate.

Generation of angiogram images

The mice perfused with Microfil were then stored overnight at 4 °C to allow the vascular contrast to polymerize. The femurs were dissected and fixed in 4% PFA for another 24 h. X-rays of the samples were then taken to visualize the femur and the vascular contrast (Supplemental Fig. 1b). The femur was placed in 0.5 M EDTA pH 8 for decalcification then imaged via X-ray (Supplemental Fig. 1c). The muscles surrounding the femur were removed, and the leg was photographed and X-rayed (Figs. 1d & e). Demineralized specimens were imaged by μCT (μCT40, Scanco-Medical-AG, Bassersdorf, Switzerland) with a 20 μm isotropic

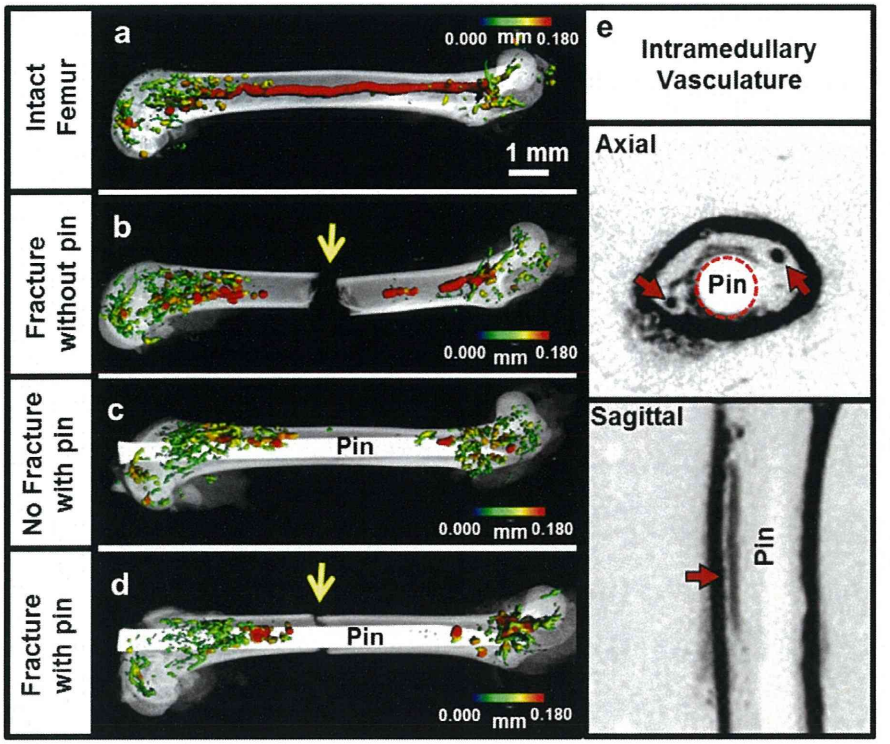

Fig. 1. Fracture and/or intramedullary reaming produce a segmental avascular diaphyseal segment. (a) Femoral angiography reveals larger unbranched vasculature within the diaphysis and smaller branched vasculature within the proximal and distal metaphysis. (b) Immediately following a fracture (yellow arrow) angiography demonstrates a segmental diaphyseal avascular segment approximately 1 mm proximal and distal to the injury without disruption of the metaphyseal vasculature. (c) Reaming and pin placement alone and (d) fracture with reaming and pin placement produce a similar diaphyseal avascular segment without disruption of the metaphyseal vasculature. (e) Two-dimensional slices from μCT demonstrate that the intramedullary pin does not prevent diaphyseal intramedullary vasculature (red arrows). Vessel diameter demarcated by color (0 and 0.18 mm) in all figures.

voxel size. A Scanco-Medical evaluation script was applied to render the vasculature with colors corresponding to vessel diameter between 0 and 0.18 mm. These vascular images were integrated into the initial X-rays by matching size and orientation using Adobe Photoshop (San Jose, CA) (Supplemental Figs. 1f–h). Quantitation of liver vasculature also demonstrates no difference in vessel volume, number, or branching (Supplemental Fig. 2b) which in combination our gross observations indicates consistent filling of the vessels with angiogram contrast.

Histology

Histologic sections prepared from PFA-fixed, demineralized in 0.5 M EDTA (pH 7.2) and paraffin-embedded specimens were cut on to slides in 5 μm sections. The slides were then deparaffinized and hydrated for use in immunohistochemistry or histological staining (Safranin-O stain). The sections were stained with Safranin-O/Fast green (Safranin-O) as previously described [46]. Briefly the slides were placed in Weigert's hematoxylin for 10 min, washed in running tap water and then stained with 0.1% fast green solution for 5 min. The slides were then rinsed for 5 s in 1% acetic acid and placed in 0.1% safranin and orange solution for 5 min. The slides were then dehydrated and coverslip for light microscopy.

Immunofluorescence microscopy

After, the slides were deparaffinized and hydrated. Sodium citrate antigen retrieval was performed using 0.1 M citric acid and 0.1 M sodium citrate. The slides were heated for 2 min in the microwave, cooled to room temperature and then washed gently with Tris buffer saline (TBS). The slides were blocked (5% BSA solution containing 10% goat serum) and immunostained with anti-mouse VEGF-A (1:200, Abcam 46154, Cambridge, MA), VEGFR2 goat anti-mouse (1:50, R&D systems AF644) or an rabbit anti-mouse VEGFR1 (1:100, Abcam 32152) antibody overnight at 4 °C. The slides were then washed and incubated with 10 μg/ml of Alexa Fluor 647-labeled anti-rabbit antibody (Life Technologies 792514, Grand Island, NY) in blocking buffer for 1 h. The slides were counterstained with DAPI and cover slipped using mounting solution (PolySciences Warrington, PA) and fluorescent images were taken (NIKON AZ100, Upright wide field microscope). The slides incubated without primary antibodies served as negative controls.

Quantification of soft and hard tissue callus size

Soft tissue callus delineated by safranin-O red staining was traced on 5 histological step-sections 200 μm apart as previously described with the following changes [50]. To determine the orientation of the 5 slides, the edge of the callus was visualized by identifying the first section with callus on both the medial and lateral femoral cortex and the middle of the callus was determined by the pin space. Each of the specimens' 5 sections were measured by 4 blinded reviewers and results were then expressed as mm^2 the soft tissue callus area. Hard tissue callus size was measured from radiographs of fractured femurs as previously described [45]. Briefly the mice were placed in the prone position and an X-ray was taken. The total area of the mineralized callus was determined each week by tracing the area of the fracture callus on X-rays by 2 reviewers and results were then expressed as mm^2 the hard tissue callus. Image quantification for both the soft and hard tissue calluses was performed using the software program ImageJ (NIH, http://rsb.info.nih.gov/ij/). Trend lines were generated between the data points using a spline curve and GraphPad prism.

Quantification of vasculature

Vessel volume was determined by μCT on the fracture callus of the demineralized femurs perfused with angiogram contrast. A cylinder comprised of 250 slices with a 20 μm isotropic voxel size was placed over the fracture callus to define the volume of interest. A threshold of 122 (lower) and 1000 (upper) was applied for segmentation with Gauss sigma of 0.8 and a gauss support of 2 to reduce the noise. Vessel volume (TRI BV) was then evaluated using Scanco μCT standard algorithms and graphed. Spline trend lines were generated between the data points using a spline curve function in GraphPad Prism 6.

Sources of funding

Caitlin Lovejoy Fund, NIH (S10 RR027631), and the Musculoskeletal Transplantation Foundation.

Results

Fracture and/or reaming disrupt diaphyseal intramedullary vascularity

Consistent with previous reports [51], the vasculature of the femoral mid-diaphysis is composed primarily of larger intramedullary vessels

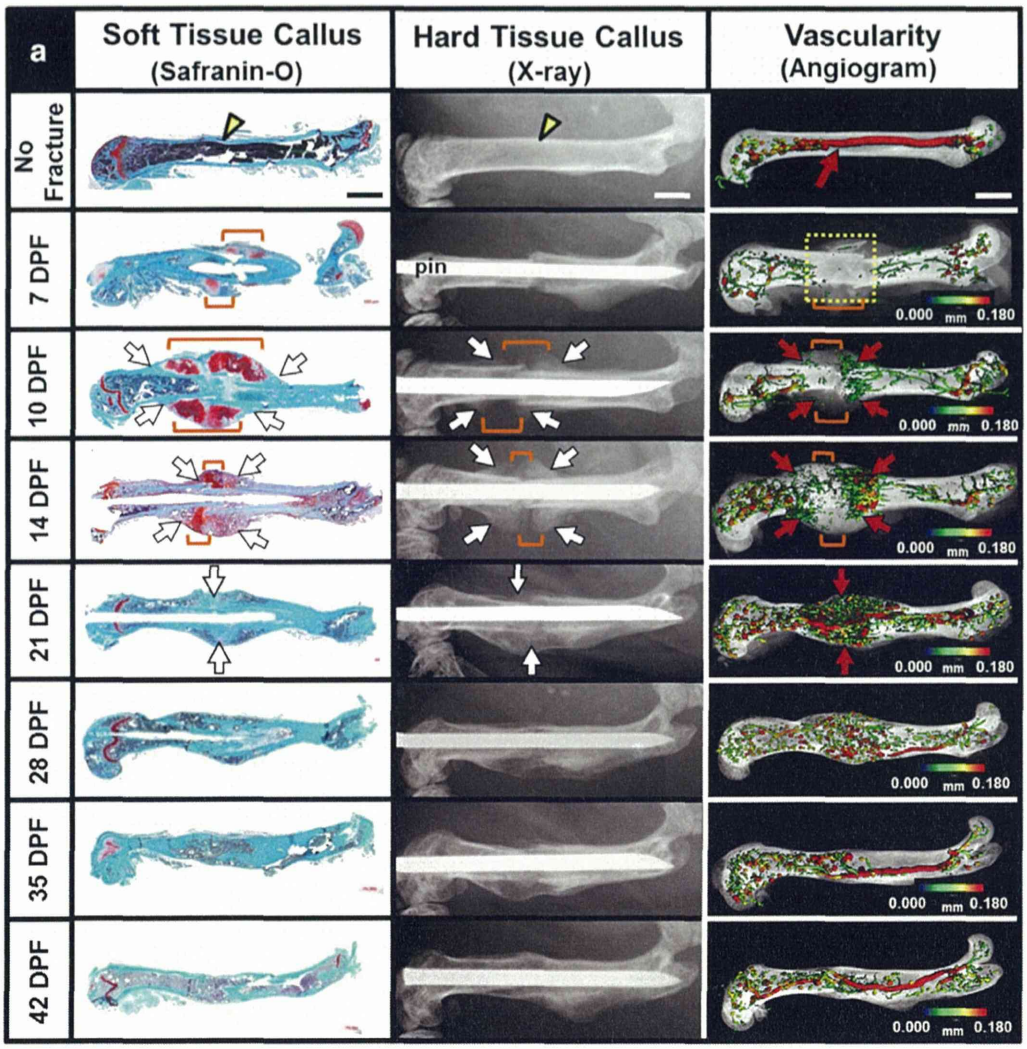

Fig. 2. Vascular development relative to soft tissue and hard tissue callus formation in a displaced, stabilized fracture. (a) Safranin-O-staining, radiographs, and angiograms were performed on fractured femurs at specified intervals following a fracture to elucidate the temporal and spatial development of the fracture callus and associated vasculature (high power images, b). Representative images are shown: quantitative measurements of the hard and soft tissue calluses and fracture vasculature are provided in Table 1 and Fig. 3. Prior to fracture (no fracture) the mid-diaphyseal segment is composed of intact cortical bone (yellow arrowhead on Safranin-O and radiograph) with intact intramedullary vasculature (red arrow on angiogram). 7 days post fracture (7-DPF), disruption of the intramedullary vascular system (yellow box on angiogram) is accompanied by the development of chondroid tissue within the avascular zone of the healing fracture (red staining on Safranin-O, orange bracket) without obvious development of hard tissue callus by radiographic examination. By 10 days post fracture (10-DPF), the soft tissue callus has grown to its maximal size (orange bracket on Safranin-O) and is largely limited to the avascular regions of the healing fracture. Small, newly formed vessels are observed (red arrows on angiogram) proximal and distal to the avascular soft tissue callus. These new vessels seem to arise directly from intact intramedullary vessels. Radiographs reveal initial formation of hard tissue callus 10 days post fracture (white arrows X-ray) overlying areas of developing vascularity, but not within avascular soft tissue callus (orange brackets). 14 days post fracture (14-DPF), newly formed extramedullary vasculature rapidly extends from the proximal and distal aspects of the fracture callus toward the center of the fracture callus (red arrows on angiogram). As the vascular network develops, the soft tissue callus is replaced by hard tissue callus (white arrows on Safranin-O and on X-ray). By 21 days post fracture (21-DPF) the fracture callus has been completely bridged by vascular anastomosis (red arrows on angiogram) which occurs contemporaneously with complete resorption of the soft tissue callus and union of hard tissue callus (white arrows on Safranin-O and X-ray). Fracture callus undergoes vascular remodeling (angiogram) together with remodeling of the hard tissue callus during the next 14 days (28-DPF through 42-DPF), restoring the femoral diaphysis to its original form. (b) Higher power magnification of the fracture callus. Images are representative sections from for each time group ($n \geq 5$). Vessel diameter demarcated by color (0 and 0.18 mm) in all figures.

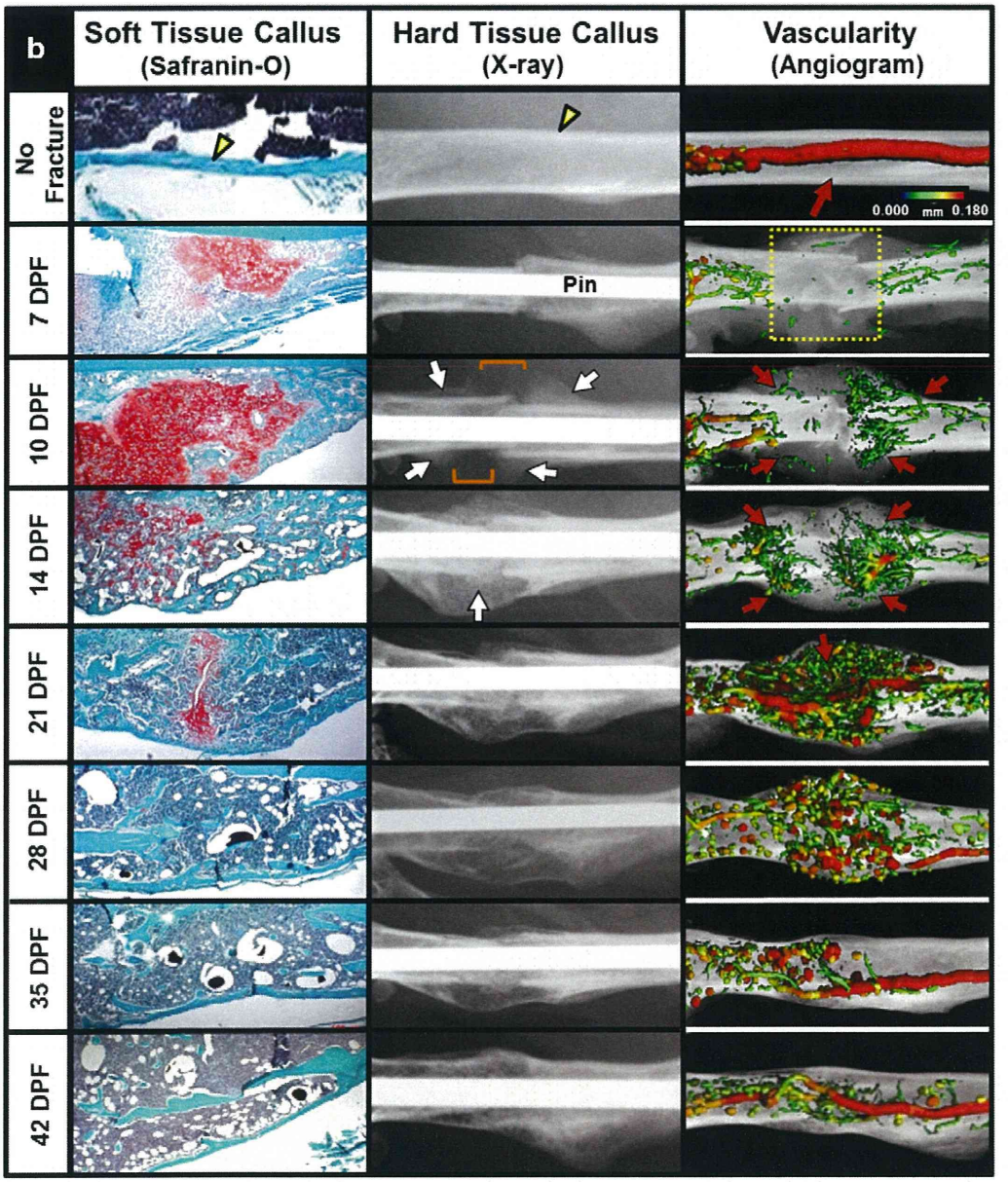

Fig. 2 (*continued*).

with few branching points. In contrast, the proximal and distal metaphysis is composed of multiple intramedullary vessels significantly smaller and with many more branching points than the diaphysis (Fig. 1a). Upon fracture the diaphyseal vascularity is disrupted at the fracture site whereas the proximal and distal metaphyseal vascularity remain intact resulting in a segmental loss of intramedullary vascularity approximately 1 mm proximal and distal to the insult (Fig. 1b) without significant disruption of metaphyseal vascularity. A similar pattern of metaphyseal sparing segmental diaphyseal avascularity occurs following an intramedullary reaming and pin stabilization without (Fig. 1c) or with (Fig. 1d) fracture. μCT angiography confirms that the 23-G intramedullary pin utilized to stable the fracture permits revascularization through the intramedullary compartment of the diaphysis (Fig. 1e).

Vascular development relative to soft tissue and hard tissue callus in a displaced fracture

Safranin-O-staining, radiographs, and angiograms of fractured femurs elucidates the temporal and spatial development of the fracture callus and associated vasculature (Fig. 2a). Seven days post-fracture (7-DPF), the diaphyseal intramedullary vasculature remains disrupted, resulting in an avascular femoral segment flanked proximally and distally by intact intramedullary vasculature. Radiographic and histopathologic examination shows formation of a cartilaginous soft tissue callus without evidence of osteoid formation within this avascular zone. The soft tissue callus rapidly enlarges to its maximal size by 10-DPF. Simultaneously, hard tissue callus is initially formed via intramembranous ossification at the extreme proximal and distal aspects

of the fracture site, where the periosteum inserts on unaffected adjacent cortical bone. This process occurs in conjunction with the formation of small highly branching extramedullary vessels (10-DPF). As hard tissue callus replaces soft tissue callus (14-DPF), it is accompanied by an expansion of newly formed vasculature. Spatially, the regions of vascular expansion begin at the proximal and distal aspects of the fracture site and migrate centrally toward the soft tissue callus. Vascular ingrowth continues until anastomoses are developed, coinciding with complete dissolution of soft tissue callus and formation of bridging hard tissue callus (21-DPF). Following a vascular anastomosis and bridging of hard callus across the fracture site, the fracture callus remodels back to within the original cortices coinciding with the vasculature returning to larger vessels with reduced branching (28–42-DPF). Higher power views of the fracture callus are presented in Fig. 2b.

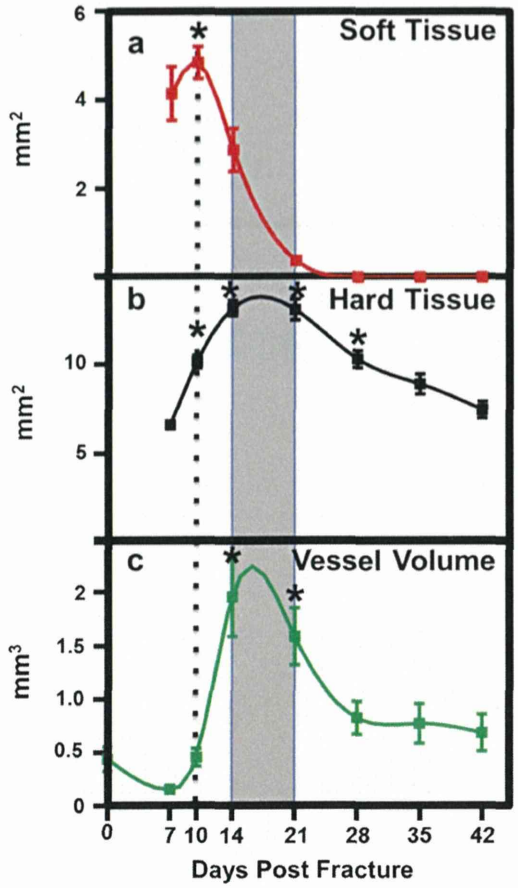

Fig. 3. Quantitation of vascular development relative to soft tissue and hard tissue callus in a displaced fracture. (a) Quantification of the soft tissue callus identified by Safranin-O staining reveals significant development of cartilage at 7–14-DPF relative to 42-DPF with maximum area at 10-DPF (hashed line). Soft tissue callus was last detected at 21-DPF. (b) Quantification of hard tissue callus identified by X-ray reveals the first significant new bone development which occurs at 10-DPF with maximum size between 14 and 21-DPF (gray zone). Hard tissue callus size subsequently remodels, decreasing in size, to its original pre-fracture size by 42-DPF. (c) Quantification of vessel volume identified by μCT of decalcified angiograms reveals an initial loss of vascularity with subsequent increase initiating at the time of maximum soft tissue callus and reaching maximum vessel volume between 14 and 21-DPF. Vessel volume then reduces from 21 to 42-DPF near the pre-fracture diaphyseal vessel volume. All samples were evaluated from 7 to 42 days following a fracture and trend lines were generated using a spline curve fit. Dotted line denotes the maximum soft tissue callus size and gray zone denotes the maximum hard tissue callus size. Statistical analyses of soft tissue callus, hard tissue callus, and vessel volume were performed using non-parametric ANOVA with a Dunn's multiple comparison test. Significance (p value < 0.1) is denoted by asterisk and all error bars represent standard error of the mean. For statistical analysis of the soft tissue callus all values were compared to 21-DPF. For statistical analysis of the hard tissue callus all values were compared to 42-DPF. For statistical analysis of vessel volume all values were compared to un-fractured femora. See Table 1 for more details.

Quantitation of angiogenesis relative to soft tissue and hard tissue callus in a displaced fracture

Relative to hard tissue callus and vascularity, the soft tissue callus is the fastest developing matrix following a fracture, reaching its maximum size by 10-DPF and decreasing in size until it is undetectable at 28-DPF (Fig. 3a). Hard tissue callus develops later than the soft-tissue callus, reaching its maximum size between 14 and 21-DPF, and then steadily returns to its initial size by 42-DPF (Fig. 3b). In accordance with our findings that fracture and insertion of an intramedullary device (Fig. 1) produce an avascular segment of diaphyseal bone around the fracture site, the average vessel volume initially decreases immediately following a fracture (Fig. 3c). At the point of maximum soft tissue callus (hashed line) vessel volume begins to increases reaching maximum volume at the same time as maximum hard tissue callus (gray zone). Vessel volume subsequently decreases approaching, but not reaching, the pre-fracture vessel volume by 42-DPF. Data used for generation of the graphs are presented in Table 1.

Newly formed subperiosteal vasculature arises from intact intramedullary vasculature

High power magnification of angiograms reveal that by 10-DPF newly formed extramedullary vasculature arises from intact intramedullary blood vessels proximal and distal to the fracture site (Fig. 4a). These intramedullary–extramedullary vascular anastomoses are also demonstrated by 2D reconstruction of μCT images and close macroscopic inspection of the cut surfaces of contrast-injected and decalcified femur fracture specimens. These data demonstrate multiple communicating vessels apparently arising from intramedullary vasculature, traversing the cortical bone and branching into numerous small vessels supplying the newly formed hard tissue callus in the subperiosteal space (Figs. 4b–f). Such anastomoses were only observed at the proximal and distal ends of the fracture callus, indicating that they were not native nutrient vessels of the femur. Axial 2D reconstructions confirm that the 23-G pin used to stabilize the fracture did not completely occlude or completely disrupt the intramedullary vasculature.

Fracture angiogenesis co-localizes with the hard tissue callus and invades the soft tissue callus

Multiple lines of evidence illustrate that the extramedullary vasculature is associated with developing hard tissue callus and resorption of soft tissue callus. Sagittal sectioning of vascular contrast-filled fracture callus (10-DPF) reveals robust development of extramedullary vasculature in hard tissue callus at the proximal and distal aspects of the

Table 1
Quantitation of fracture callus vascularity relative to the soft and hard tissue calluses throughout fracture repair.

Days post fracture	Soft tissue callus mm^2			Hard tissue callus mm^2			Vessel volume mm^3		
	Mean	SD	N	Mean	SD	N	Mean	SD	N
Intact femur	–	–	–	–	–	–	0.44	0.22	4
7	4.14	1.70	8	6.60	0.85	18	0.16	0.06	6
10	4.84	0.96	7	10.17	1.72	22	0.46	0.22	7
14	2.87	1.61	11	13.18	2.52	33	1.96	1.49	16
21	0.37	0.33	11	13.10	3.37	33	1.59	0.89	11
28	0.00	0.00	11	10.30	2.35	24	0.83	0.46	9
35	0.00	0.00	11	8.91	2.71	23	0.86	0.48	5
42	0.00	0.00	11	7.45	2.02	19	0.69	0.35	4

N = number of samples, SD = standard deviation.